Liquid-Solid Mass Transfer in Conventional and Inverse Fluidized Beds

by

Victer Veldman

Dissertation presented in partial fulfilment of the requirements
for the degree of
Master of Engineering in Chemical Engineering
at the University of Pretoria

Faculty of Engineering, the Built Environment and Information Technology
Department of Chemical Engineering
University of Pretoria

Supervisor: Prof. W. Nicol

November 2012

Synopsis

Liquid-solid mass transfer was experimentally determined on a novel reactor, with external recycling. Liquid-solid experiments were performed in both up-flow and down-flow mode depending on the particle density. In addition, three-phase experiments were performed in concurrent up-flow mode. The dissolution of benzoic acid method was adapted and used in order to quantify the liquid-solid mass transfer rate.

It was found that the direction of liquid flow had no influence on liquid-solid mass transfer for two-phase fluidized beds. It was, however, found that the density difference between the solid particle and liquid (Δρ) had a significant influence on the liquid-solid mass transfer. For higher Δρ, higher mass transfer coefficients were achieved. The liquid-solid mass transfer coefficient increased until minimum fluidization was reached, after which the increase in mass transfer was less severe with a further increase in liquid velocity.

The correlation proposed by Kawase and Moo-Young (1987) effectively fits the experimental data from the minimum fluidization velocity (u_{mf}) until the onset of turbulent velocity (u_c). This correlation exhibits an absolute average relative error (AARE) of 18% when the data points for all four particles are compared with the correlation. A new correlation is proposed with the inclusion of the dimensionless group, the Archimedes number. The correlation proposed achieved an AARE of only 8%, and can be seen in the equation below.

$$Sh = 0.05Re^{0.42}Sc^{0.66}Ar^{0.17}$$

A comparison between fluidized bed performance and packed bed performance showed that the density difference determines the superior mode of liquid-solid mass transfer. When Δρ is high, as for the alumina particles Δρ = 1 300 kg/m^3, the fluidized bed outperforms the packed bed. When the density difference becomes smaller, Δρ = 580 kg/m^3, the fluidized

bed only slightly outperforms the packed bed setup, while for a very small density difference ($\Delta\rho$ = -145 kg/m^3) the packed bed substantially outperforms the fluidized bed. This trend is irrespective of the direction of fluidization. When $\Delta\rho$ is negative it indicates inverse fluidization.

With the introduction of gas to the system, higher liquid-solid mass transfer coefficients were obtained at the same superficial liquid velocity. Furthermore, no significant transitions were seen between the minimum fluidization and the onset of turbulence flow regimes, as seen with two-phase fluidization. This contributed to the gradual fluidization that was seen with three-phase fluidization and not instantaneous fluidization, as with liquid-solid fluidized beds.

Keywords: Liquid-solid mass transfer, inverse fluidization, conventional fluidization

Table of Contents

List of Figures

List of Tables

Nomenclature

Symbol	Description	Units
a_s	Total external area of coated particles	m^2
A_{col}	Area of column	m^2
Ar	Archimedes number	-
C_{Ab}	Concentration of benzoic acid in water	kg/m^3
C_{sat}	Saturation concentration of benzoic acid in water at 30 ^oC	kg/m^3
C_v	Volumetric solid concentration	v/v
C_{PC}	Concentration at which partial coverage occurs	g/l
C_{max}	Maximum concentration possible inside reactor	g/l
d_*	Dimensionless particle diameter	-
d_o	Diameter of orifice in sparger	mm
dp	Particle diameter	m
D_C	Column diameter	m
D_l	Axial dispersion coefficient	m^2/s
e	Energy dissipated per unit mass of liquid	m^2/s^2
F_B	Bubble frequency	-
H_{bed}	Bed height	m
K_d	Distributor coefficient	-
k_s	Liquid-solid mass transfer coefficient	m/s
L_v	Bubble size	m
N_o	Number of orifices in sparger	-
P_T	Total pressure	kg/ms^2
P_S	Vapour pressure of liquid	kg/ms^2
Pe	Peclet number	-
Re_c	Reynolds number at u_c	-
Re_{lmfo}	Reynolds number at minimum fluidization with no gas flow	-
Re_{mf}	Reynolds number at minimum fluidization	-
$Re_{t\infty}$	Reynolds number of one particle in infinite medium	-

Sc	Schmidt number	-
Sh	Sherwood number	-
Sh_{FB}	Sherwood number for fluidized bed	-
Sh_{PB}	Sherwood number for packed bed	-
Sh_{exp}	Experimentally determined Sherwood number	-
u_*	Dimensionless terminal velocity	-
u_c	Onset of turbulent regime liquid velocity	m/s
u_{mf}	Minimum fluidization velocity	m/s
u_g	Superficial gas velocity	m/s
u_l	Liquid superficial velocity	m/s
u_t	Terminal velocity	m/s
U_B	Bubble rise velocity	m/s
vvm	Volume of gas fed to reactor per volume of reactor per minute	ml/ml.min
V	Volume of reactor	m^3
V_{samp}	Volume of samples taken	m^3

Greek Symbols

α	Equation constant in Equation (2.32)	-
β	Equation constant in Equation (2.32)	-
γ	Equation constant in Equation (2.32)	-
ε	Void fraction	-
ε_g	Gas hold-up	-
μ_l	Liquid viscosity	Pa.s
ρ_l	Liquid density	kg/m^3
ρ_g	Gas density	kg/m^3
Δρ	Density difference between liquid and solid phases	kg/m^3
Δz	Distance between measuring points	mm
Φ	Sphericity	-
ν	Kinematic viscosity	m^2/s

1. Introduction

Fluidized beds are used extensively in practice, especially gas-phase conventional (up-flow) fluidization. Applications of three-phase fluidized beds include gas-liquid reactions where a solid catalyst is required. Such processes include petrochemical processes such as hydrogenation, wastewater treatment, the Fisher-Tropsch process and fermentation (Kim and Kang; 1997). Liquid-solid two-phase fluidization is less renowned but is still widely used in industry for sedimentation, catalytic cracking, ion exchange, etc. (Roy and Dudukovic; 2001, Fan; 1989). Inverse fluidization (down-flow of liquid) differs from conventional fluidization (up-flow of liquid) in the sense that the particles have a lower density than the carrier fluid. Fluidization is achieved by overcoming the buoyant forces through a constant down-flow of the carrier fluid. Inverse fluidized beds (IFB) have been used in practice for many biochemical applications such as aerobic and anaerobic water treatment plants and processes such as ferrous iron oxidation (Nikolov and Karamanev; 1987). It is speculated by Renganathan and Krishnaiah (2005) that inverse fluidization holds numerous advantages over classical fluidization. These advantages include: less solids attrition, less carry-over of coated microorganisms, ease of re-fluidization and effective control of biofilm thickness.

For the successful design, analysis and operation of any reactor, extensive knowledge is required of the hydrodynamics of the reactor. To date the hydrodynamic investigations on inverse fluidized beds involved the minimum fluidization velocity (Renganathan and Krishnaiah, 2003), the gas hold-up (Fan, Muroyama and Chern, 1982 and Myre and Macchi, 2010), two-phase residence time distribution (Renganathan and Krishnaiah, 2004) and bubble properties (Son, Kang, Kim, Kang and Kim, 2007). No studies on liquid-solid mass transfer and gas-liquid mass transfer for inverse fluidized beds have been done to date; however, numerous studies on conventional fluidization have been performed (Arters and Fan, 1990).

The objective of the present study was to quantify and model the liquid-solid mass transfer coefficient for two-phase fluidization in both liquid up-flow and down-flow modes. Different particle densities were used in an aqueous medium, resulting in a

density difference between the solid and the liquid. A comparison was done between four different particle types ($\Delta \rho$ between 410 kg/m^3 to 1 300 kg/m^3) in order to determine the effect on liquid-solid mass transfer. These results could then be compared to a packed bed setup. The effect of a gas-phase inclusion on a conventional liquid-solid fluidized bed was also investigated in order to compare liquid-solid mass transfer coefficients between three-phase fluidization and a conventional liquid-solid fluidization. An increase in reactor performance with an inclusion of a gas phase was expected, as reported by Arters and Fan (1990).

Experimental work was performed on a novel reactor with external recycling. Liquid-solid experiments were performed in both up-flow and down-flow mode depending on the particle density. In addition, three-phase experiments were performed in concurrent up-flow mode. The dissolution of benzoic acid method was implemented in order to quantify the liquid-solid mass transfer rate. The liquid-solid mass transfer coefficient was experimentally determined over a wide range of liquid velocities in order to investigate bed behaviour. Modelling was done on the data generated in order to compare the results with the literature correlations and develop new correlations.

2. Transport Parameters Prediction

A survey was done on fluidized bed studies done in literature in order to have a background on expected fluidization hydrodynamics. As a starting point liquid-solid conventional fluidized beds will be discussed. Inverse liquid-solid fluidized bed studies were also investigated in order to examine possible variations from conventional fluidization. The inclusion of a gas phase to both conventional and inverse fluidized beds was also investigated. Lastly an investigation was done on all liquid fluidization liquid-solid mass transfer studies, in order to compile expected trends along with literature correlations.

2.1 Liquid-solid conventional fluidized bed hydrodynamics

Two-phase conventional fluidized beds have been extensively covered in the literature. When the hydrodynamics of a fluidized bed are investigated, a key influencing factor is the contacting regime the bed is operating under. For liquid fluidization the regimes become more limited (when compared to gas fluidization), with the three most prominent regimes being fixed bed, minimum fluidization and smooth fluidization, as shown in Figure 2.1.

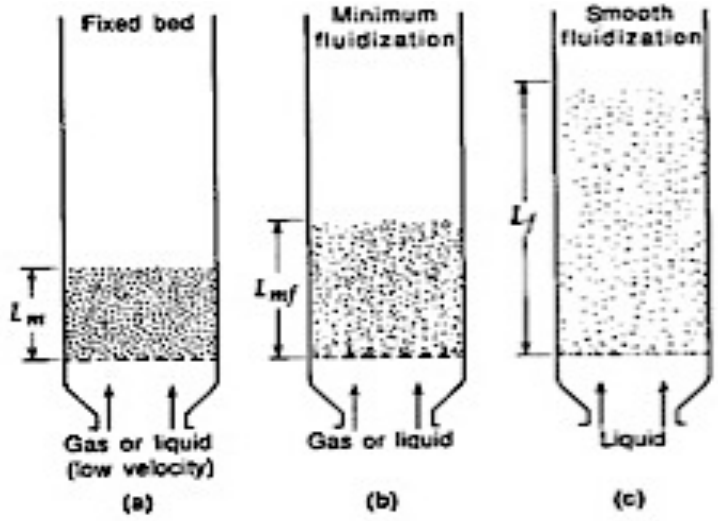

Figure 2.1: Various contacting regimes in liquid fluidization (Kunii & Levenspiel, 1999: 2)

1.1.1 Minimum fluidization velocity (MFV)

In liquid-solid fluidization the onset of fluidization occurs when the particles become suspended in the fluid (Niven, 2002). The pressure loss can then be given by Equation (2.1). When this equation for the pressure loss is combined with the Ergun equation, an expression is found for the minimum fluidization velocity in terms of Re_{mf} (Equation 2.2). (Wen and Yu, 1966).

$$\frac{\Delta P}{L} = \left(1 - \varepsilon_{mf}\right)\left(\rho_s - \rho_f\right)g \tag{2.1}$$

$$\frac{1.75}{\varphi_p {\varepsilon_{mf}}^3} {Re_{mf}}^2 + \frac{150(1-\varepsilon_{mf})}{{\varphi_p}^2 {\varepsilon_{mf}}^3} Re_{mf} - Ar = 0 \tag{2.2}$$

Where φ_p is the particle shpericity. The void fraction itself is a function of velocity; therefore Wen and Yu (1966) experimentally determined approximations for the voidage functions (Equations 2.3 and 2.4). Inclusion of these approximations in Equation (2.2) yields a simplified equation for the calculation of Re_{mf} that can be seen in Equation (2.5). This is the so-called 'Wen and Yu equation'.

$$\frac{1}{\varphi_p {\varepsilon_{mf}}^3} \approx 14 \tag{2.3}$$

$$\frac{(1-\varepsilon_{mf})}{{\varphi_p}^2 {\varepsilon_{mf}}^3} \approx 11 \tag{2.4}$$

$$Re_{mf} = \sqrt{33.7^2 + 0.0408\, Ar} - 33.7 \tag{2.5}$$

1.1.2 Void fraction

The average void fraction is a parameter used to quantify bed expansion. Bed expansion is one of the most important constraints when designing a reactor because it gives an indication of the bed height under operation.

Numerous correlations based on separate studies have been proposed, but the correlation proposed by Richardson and Zaki (1954) remains popular because of its simplicity – this can be seen in Equation (2.6). The exponent n can be calculated from Equations 2.7 – 2.11.

$$\left(\frac{u_l}{u_t}\right) = \varepsilon^n \tag{2.6}$$

$$n = 4.65 + 20\frac{d_p}{D}, \qquad Re_{t\infty} < 0.2 \tag{2.7}$$

$$n = \left(4.4 + 18\frac{d_p}{D}\right) Re_{t\infty}{}^{-0.03}, \qquad 0.2 < Re_{t\infty} < 1 \tag{2.8}$$

$$n = \left(4.4 + 18\frac{d_p}{D}\right) Re_{t\infty}{}^{-0.1}, \; 1 < Re_{t\infty} < 200 \tag{2.9}$$

$$n = (4.4) Re_{t\infty}{}^{-0.1}, \quad 200 < Re_{t\infty} < 500 \tag{2.10}$$

$$n = 2.4\,, \qquad 500 < Re_{t\infty} \tag{2.11}$$

The terminal velocity for a single particle (u_t) can be found using Equation (2.12) (Khan and Richardson, 1990).

$$\left(\frac{u_t}{u_{t\infty}}\right) = 1 - 1.15\left(\frac{d_p}{D}\right)^{0.6} \tag{2.12}$$

By using the standard drag law, $u_{t\infty}$ can be calculated (Richardson and Zaki, 1954). This approach of calculating the terminal velocity takes into account wall drag effects but it is not repeatable for all systems.

1.2 Liquid-solid-gas conventional fluidization hydrodynamics

1.2.1 Minimum fluidization velocity (MFV)

In three-phase fluidization the addition of a gas phase adds numerous complications to the fluidization. Zhang et al. (1995) developed a model that takes into account all the added effects of the gas-phase, namely the gas-perturbed liquid model (GPLM). This model equates the liquid-buoyed weight of solids per unit bed volume to the frictional pressure gradient given by the Ergun packed bed equation applied to the liquid-solids part of the incipiently fluidized bed. By using similar approximations to those made by Wen and Yu (1966), Zang et al. (1995) simplified the model to Equation (2.13).

$$Re_{lmf} = \sqrt{33.7^2 + 0.0406Ar\left(1-\alpha_{mf}\right)^3} - 33.7 \tag{2.13}$$

where α_{mf} is the gas hold-up divided by the total liquid hold-up, including the liquid trapped in the gas phase, at minimum fluidization.

Yang et al. (1993) developed a good estimation of α_{mf} for co-current upward flow of gas in a non-foaming liquid. This estimation can be seen in Equation (2.14).

$$\alpha_{mf} = \frac{0.16U_g}{\varepsilon_{mf}(U_g+U_{lmf})} \tag{2.14}$$

1.2.2 Gas hold-up

Fan, Muroyama and Chern (1982) did a study on gas hold-up for two different flow regimes in inverse fluidized beds. For every superficial gas velocity (U_{g0}) a gas hold-up (ε_g) was measured and documented. They used this data to compile two empirical equations. These two equations can be seen in Equation (2.15) (inverse bubbling fluidized bed regime) and Equation (2.16) (inverse slugging fluidized bed regime).

$$\varepsilon_g = 0.322\, e^{1.35}\left(\frac{U_{g0}}{U_{l0}}\right)^{0.18} \tag{2.15}$$

$$\varepsilon_g = 2.43\, {U_{g0}}^{0.704} {U_{l0}}^{0.25} \tag{2.16}$$

Myre and Macchi (2010) expanded the work done by Fan, Muroyama and Chern (1982) in order to apply it to a wider range of physical parameters. The authors built an acrylic column with a height of 2.15 m and a diameter of 0.152 m, which can be operated as either a bubble column with no particles or as an inverse fluidized bed with particles in order to determine the effects of gas flow rate, liquid flow rate and particle loading on the gas hold-up in the column. Myre and Macchi (2010) found that the gas hold-up decreased with an increase in solids loading. This was attributed to an increase in bubble coalescence caused by the particles, which means that fewer micro bubbles are present.

Myre and Macchi (2010) adapted the correlation proposed by Bekish et al. (2006) for the prediction of gas hold-up. Myre and Macchi (2010) adapted the model by changing the leading constant parameter from 4.94 x 10^{-3} to 8.74 x 10^{-3}. The modified correlation can be seen in Equation (2.17). This modification decreased the AARE value from 42% to 9%.

$$\varepsilon_G = 0.00494\, A\, B\, C \tag{2.17}$$

With:

$$A = \left(\frac{{\rho_L}^{0.415}{\rho_G}^{0.177}}{{\mu_L}^{0.174}{\sigma_L}^{0.27}}\right){U_G}^{0.553}\left(\frac{P_T}{P_T - P_s}\right)^{0.203}$$

$$B = \left(\frac{D_c}{D_c + 1}\right)^{-0.117} \Gamma^{0.053}$$

$$C = \exp\left[-2.231C_v - 0.157\left(\rho_p d_p\right) - 0.242X_W\right]$$

$$\Gamma = (K_d \times N_0 {d_0}^{\alpha}) \quad (2.18)$$

Where

C_V is the volumetric solid concentration in the slurry (v/v),

P_T is the total pressure,

P_s is the vapour pressure of the liquid and

D_C is the column diameter (m).

The effect of the gas sparger is introduced to the correlation by Γ and can be calculated by using Equation (2.18), where

K_d is the distributor coefficient,

N_0 is the number of orifices in the sparger and

d_0 is the diameter of the orifice.

K_d values for perforated plates and multiple-orifice nozzles are 1.364.

1.2.3 Bubble properties

Son, Kang, Kim, Kang and Kim (2007) did a study on bubble size, bubble rise velocity and bubble frequency in an inverse fluidized bed using a dual electrical resistivity probe system. These parameters were measured for different liquid viscosities by using aqueous solutions of carboxyl methyl cellulose (CMC). The authors used two types of particles, polypropylene and polyethylene, with densities of 877.3 kg/m^3 and 966.6 kg/m^3, respectively. The data were generated using a dual electrical resistivity probe system. The following results were obtained:

- The bubble size was correlated using the cord length of the bubbles. It was found that the cord length increased with an increase in gas velocity. This was attributed to a higher bubble coalescence, which caused bigger bubble sizes. The increase in liquid velocity also caused more bubble coalescence because of the counter-flow of the liquid.
- The authors also noted that the bubble sizes were higher when polypropylene particles were used than when polyethylene particles were used. A conclusion was made that the bubble size decreases with increasing fluidized particle density in inverse fluidized beds.
- The bubble rise velocity increased with an increase in gas velocity or liquid viscosity, but decreased slightly with an increase in liquid velocity. This was attributed to the liquid drag on the bubbles.
- The bubble frequency increased with an increase in liquid or gas velocities. This influenced the gas hold-up in the column. The bubble frequency, however, decreased with an increase in liquid viscosity.
- The bubble frequency was higher for beds with heavier particles (polyethylene) than lighter particles (polypropylene).

Son et al. (2007) correlated models for the bubble size (L_v), rising velocity (U_B) and the bubble frequency (F_B) using the concept of gas drift flux. These correlations fit their data, with each equation having a correlation coefficient of between 0.90 and 0.96, and can be seen in Equations (2.19), (2.20) and (2.21) below.

$$L_v = 0.117 \left(\frac{U_G+U_L}{1-\varepsilon_G}\right)^{0.446} \left(\frac{\rho_S}{\rho_L}\right)^{-2.78} (\mu_L)^{0.191} \quad (2.19)$$

$$U_B = 0.108 \left(\frac{U_G+U_L}{1-\varepsilon_G}\right)^{-0.219} \left(\frac{\rho_S}{\rho_L}\right)^{-2.89} (\mu_L)^{0.076} \quad (2.20)$$

$$F_B = 30.846 \left(\frac{U_G+U_L}{1-\varepsilon_G}\right)^{0.404} \left(\frac{\rho_S}{\rho_L}\right)^{6.732} (\mu_L)^{-0.002} \quad (2.21)$$

1.3Inverse fluidization hydrodynamics

Inverse fluidization differs from classical fluidization in the sense that the particles have a lower density than the carrier fluid and therefore floats. A continuous downward flow of liquid then fluidizes the bed. In three-phase fluidization a gas flow is introduced in a counter flow manner. An inverse fluidized bed can also be run in liquid batch mode where there is no liquid flow and only upward gas flow through the liquid and particle bed.

1.3.1 Minimum fluidization velocity

Liquid-solid fluidization

In liquid-solid inverse fluidization, fluidization will commence once the pressure drop over the reactor is equal to the net buoyant force per unit area. The pressure drop over the bed is well correlated by the Ergun equation and therefore the MFV can be determined. Renganathan and Krishnaiah (2003) did a study of all the factors influencing the minimum fluidization velocity (MFV) in up-flow and down-flow fluidized beds to determine whether conventional fluidization correlations can be used for inverse fluidized beds.

To generate experimental data they constructed an inverse fluidized bed and measured the pressure drop and the void fraction. The MFV was then determined when the pressure drop and void fraction were plotted against liquid velocity, and an intersection point was reached between the packed bed regime and fluidized bed regime. These data were tested against correlations from the literature on conventional fluidization (Fan et al., 1982; Legile et al, 1992; Nikolov & Karamanev,1987; Krishnaiah et al., 1993; Ulganathan & Krishnaiah, 1996; Ibrahim et al., 1996; Biswas & Ganguly, 1997; Calderon et al., 1998; Banerjee et al., 1999; Buffière & Moletta, 1999; Vijayalakshmi et al., 2000; Cho et al., 2002).

The constant values in the Ergun equation have been determined in the literature by different authors under different conditions. The correlation found by Wen and Yu

(1966) for conventional fluidized beds was deemed the best when compared to the data compiled by Renganathan and Krishnaiah (2003) with an RMS error of 24 %. The equation proposed by Wen and Yu (1966) can be seen in Equation (2.22). This correlation was tested for a variety of particles.

$$Re_{lmf0} = \sqrt{33.7^2 + 0.0408Ar} - 33.7 \quad (2.22)$$

From Equation (2.22) the MFV can be calculated, where Re_{lmf0} is the Reynolds number at minimum fluidization velocity for liquid-solid fluidization, therefore it can be seen that the conventional Wen and Yu equation can be used, within an acceptable error, to calculate MFV values for IFB. This equation can be used safely over the range of Re_{lmf0} = 0.01 to 2000 and Ar = 20 to 70 x 10^6.

Liquid-solid-gas fluidization

For three-phase inverse fluidization the gas-phase is introduced in a concurrent manner to the liquid flow. This is different from conventional three-phase fluidized beds where the gas and liquid flow in a co-current manner. Renganathan and Krishnaiah (2003) studied three-phase inverse fluidization to see how the results compare to those of conventional fluidized beds. One of the main differences that the authors noticed was that the bed fluidizes gradually, unlike two-phase fluidization. The authors attributed the gradual fluidization to the recirculation of the liquid at the top of the bed due to the gas flow. This is different from conventional fluidized beds where the bed is fluidized sharply.

The gas introduced from the bottom of the column adds different effects to the fluidization. The gas reduces the effective density of the liquid and therefore the particles become less buoyant. The gas flow also causes liquid circulations in the liquid phase, which in turn causes an extra drag force on the particles.

Due to the effects discussed above, conventional fluidized bed correlations for the minimum fluidization velocity cannot be used for inverse fluidized beds. Renganathan and Krishnaiah (2003) correlated a new empirical equation for the

minimum fluidization velocity and tested it against literature correlations. The GPLM developed by Zhang et al (1995) and discussed in Section 2.2.1, was modified by Renganathan and Krishnaiah (2003) in order to apply it to inverse fluidized beds. The modified GPLM can be seen in Equations (2.23) and (2.24). Table 2.1 was compiled with empirical models as well as modified gas-perturbed liquid models. Both models can be used to predict the MFV for three-phase fluidization.

$$Re_{lmf0} = \sqrt{33.7^2 + 0.0408ArP} - 33.7 \tag{2.23}$$

$$P = \left(1 - {\alpha_{mf}}^3\right) = 1 - 7.89Ar^{-0.208}{Re_g}^{0.299} \tag{2.24}$$

Table 2.1: Models for minimum fluidization velocities in three-phase inverse fluidization including the root-mean-square (RMS) error for each.

Range Ar x 10^4	Empirical Equation	RMS Error %	Modified GPLM Re_{lmf}	RMS Error %
Low 1.47 – 8.47	$Re_{lmf} = Re_{lmf0} - 0.176Ar^{0.434}Re_g^{0.669}$	29	$\sqrt{33.7^2 + 0.0408Ar(1 - 21.2Ar^{-0.292}{Re_g}^{0.549})} - 33.7$	30
Medium 9.97 - 151	$Re_{lmf} = Re_{lmf0} - 0.0692Ar^{0.438}Re_g^{0.839}$	14	$\sqrt{33.7^2 + 0.0408Ar(1 - 1.181Ar^{-0.097}{Re_g}^{0.586})} - 33.7$	16
High 294 - 1472	$Re_{lmf} = Re_{lmf0} - 0.00185Ar^{0.578}Re_g^{0.882}$	11	$\sqrt{33.7^2 + 0.0408Ar(1 - 0.152Ar^{-0.0111}{Re_g}^{0.555})} - 33.7$	13

1.3.2 Void fraction

Renganathan and Krishnaiah (2005) set out to find a unified correlation for conventional and inverse fluidized beds by looking deeper into void fluctuations. As a starting point for their correlation they used the correlation proposed by Richardson and Zaki (1954) because of its simplicity (Equation 2.6).

This approach of calculating the terminal velocity takes into account wall drag effects, but it is not repeatable for all systems. These equations were tested for a number of experimental data and it was found that the Richardson and Zaki equation works well if experimental terminal velocities are used but not if Equation (2.12) is used. By modifying the Turton and Clark (1987) equation for terminal velocity, the overall void prediction was improved. The equation proposed by Renganathan and Krishnaiah (2005) can be seen in Equation (2.25). This equation was compared to experimental terminal velocities and an RMS error of 12% was found.

$$u_* = \left[\left(\frac{18}{{d_*}^2}\right)^{0.776} + \left(\frac{3 \times 0.571}{4{d_*}^{0.5}}\right)^{0.776}\right]^{-1/0.776} \tag{2.25}$$

where u_* is the dimensionless terminal velocity in infinite medium, and can be expressed as Equation (2.26). Similarly d_* is the dimensionless particle diameter that can be calculated using Equation (2.27).

$$u_* = u_{t\infty}\left[\left(\frac{{\rho_l}^2}{g\mu_l(\rho_l - \rho_p)}\right)\right]^{\frac{1}{3}} \tag{2.26}$$

$$d_* = d_p\left[\left(\frac{g\rho_l(\rho_l - \rho_p)}{{\mu_l}^2}\right)\right]^{\frac{1}{3}} \tag{2.27}$$

1.3.3 Liquid mixing (dispersion)

RTD (Residence time distribution) studies have been done by Renganathan and Krishnaiah (2004) on a two-phase IFB in order to quantify the extent of mixing in these reactors. It is to be expected that the extent of mixing will be higher when the liquid flow rate is higher. The RTD for a set of parameters can be seen in Figure 2.2.

By using the RTD data the liquid phase axial dispersion coefficient can be obtained by using Equation (2.28), where Δz is the distance between measuring points.

$$D_l = \frac{u_1 \Delta z}{Pe\ \varepsilon} \tag{2.28}$$

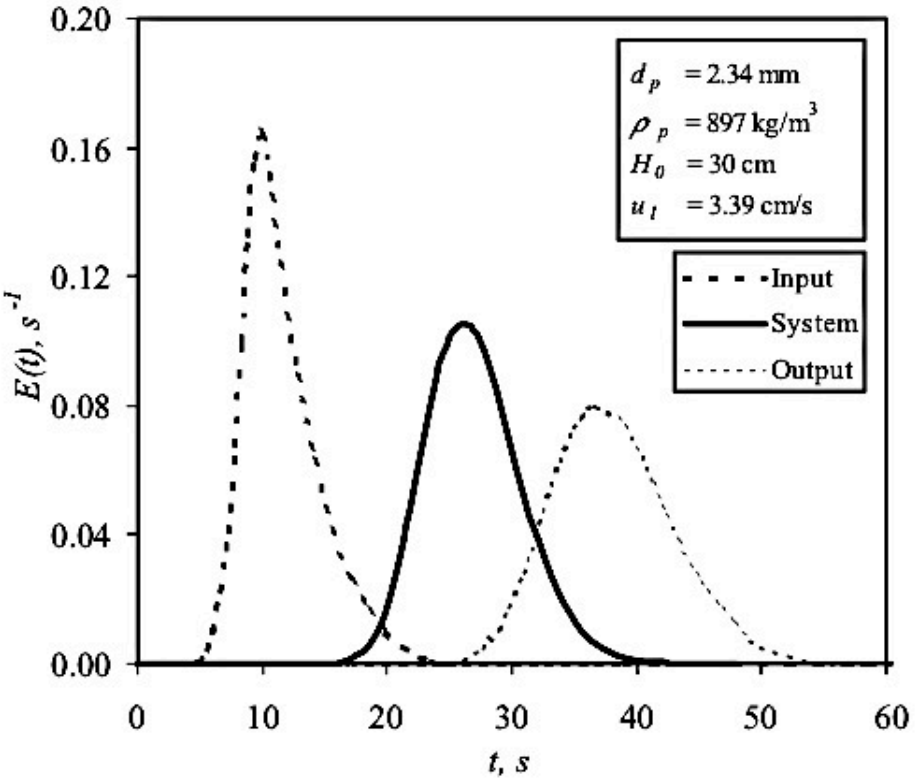

Figure 2.2: The measured input and output RTD along with the deconvoluted system RTD for a set of parameters

The authors also found that the following trends can be expected:

- The axial dispersion coefficient increases with an increase in liquid velocity. This is due to the fact that with an increase in the liquid velocity the particles move around more turbulently and therefore there is more mixing in the liquid phase.
- The dispersion coefficient stays unchanged if the static bed height is increased. This was expected because when one looks at Equation (2.28), if the static bed height is increased the Pe number increases but the expanded bed height also increases and therefore the axial dispersion coefficient will remain constant.
- If the Archimedes number is increased, the minimum fluidization velocity also increases.

In their experiments, Renganathan and Krishnaiah (2004) found a correlation for the axial dispersion coefficient that can be seen in Equation (2.29). When compared to experimental data, an RMS error of 28% was found. This correlation is only valid for $17.6 < Ar < 1.47 \times 10^7$ and $0.036 < Re < 1\,267$.

$$D_l = 1.48 \times 10^{-4} Ar^{0.66} \left(\frac{Re}{Re_{mf}}\right)^{1.73} \tag{2.29}$$

1.4Liquid-solid mass transfer in two- and three-phase fluidized beds

In any fluidized bed, whether liquid-solid or liquid-solid-gas, liquid-solid mass transfer can become a limiting step, especially for larger particle sizes. For this reason proper prediction of the liquid-solid mass transfer is needed for a proper reactor design. In order to predict the mass transfer coefficient all the factors influencing mass transfer must be investigated and understood.

According to Arters and Fan (1990) and numerous other references, the following trends can be expected in a conventional fluidized bed:

- The liquid velocity has no effect on the liquid-solid mass transfer coefficient for fully fluidized beds. This is observed in both two- and three-phase fluidization. (Hassanien et al., 1984; Arters and Fan, 1986; Prakash et al., 1987)
- The mass transfer coefficient increases at near-minimum fluidization liquid velocities. (Nikov and Delmas, 1987).
- The mass transfer is further increased as gas is introduced. This positive effect on the mass transfer tails off at higher gas velocities. These trends can be seen in Figure 2.3.
- The effect of the changing gas hold-up, because of the surfactant effect of benzoic acid, was found to have less than 15% effect on the mass transfer coefficient under normal operating conditions.
- When the effect of different inert particles was investigated it was found that when all the active and inert particles (with the same physical properties) are

completely mixed the mass transfer is not influenced by different inert particles.

Arters and Fan (1990) also investigated the effect of particle tethering. It was found that tethering of any kind affects the mass transfer when compared to free-floating particles. They also found that the mass transfer differed in the centre of the column compared to the wall: free-floating particles experience the highest mass transfer in the centre of the column and a lower mass transfer along the wall. A tethered particle only experiences one position.

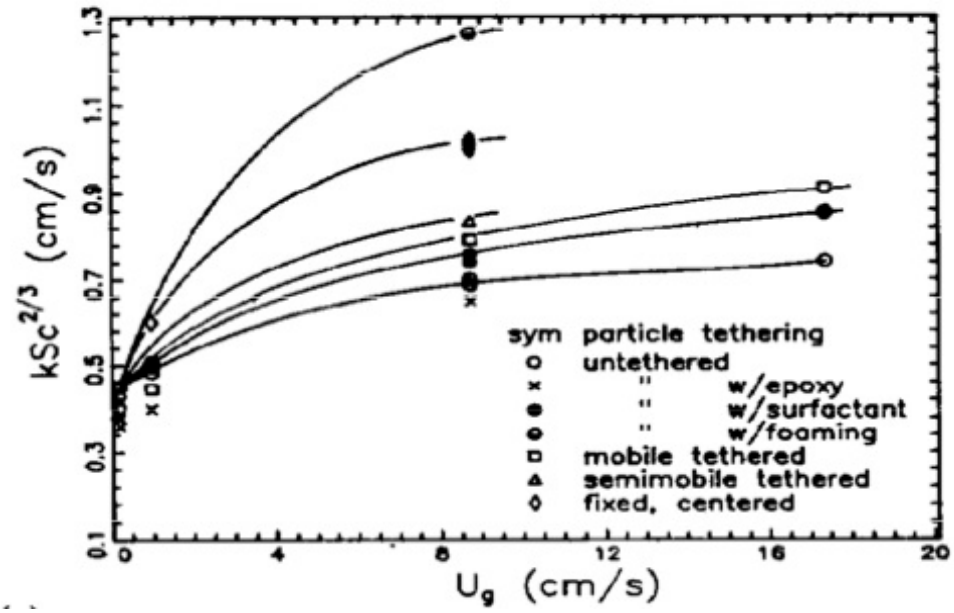

Figure 2.3: Trends observed by Arters and Fan (1990), which show an increase in mass transfer as gas velocity is increased

1.4.1 Literature correlations

No studies are found in the literature as yet on inverse fluidized beds, although conventional fluidized beds have been researched extensively. Numerous studies use energy dissipation as a starting point for their correlations (Arters and Fan, 1986; Kawase and Moo-Young, 1987; Fukuma at al., 1988; Kikuchi et al., 1983). In order to calculate the amount of energy dissipated, a three-phase system is considered. The energy balance that results from subtracting the potential energy gained by the fluid

phase from the total energy input into the system, is given by Equation (2.30) (Arters and Fan, 1990):

$$E = A_{col}H_{bed}g\left(U_l + U_g\right)\left(\varepsilon_s\rho_s + \varepsilon_l\rho_l + \varepsilon_g\rho_g\right) - A_{col}H_{bed}g\left(U_l\rho_l + U_g\rho_g\right) \quad (2.30)$$

Equation (2.30) can be simplified to Equation (2.31) using the following simplifications:

$$\rho_g \ll \rho_l, \rho_s$$

$$M_l = A_{col}H_{bed}\varepsilon_l\rho_l$$

$$e = g\left\{\left(U_l + U_g\right)(\varepsilon_s\rho_s + \varepsilon_l\rho_l) - (U_l\rho_l)\right\}/(\varepsilon_l\rho_l) \quad (2.31)$$

where e is the rate of energy dissipated per unit mass of liquid. Other studies use a less rigorous method as proposed by Fukuma et al. (1988) of determining the energy dissipated by considering the individual energy effects of the particles and the bubbles, including wall friction. Arters and Fan (1990) found this method to be just an approximation of the dissipation energy, and the method described in Equation (2.31) was found to be more accurate.

Numerous correlations found in the literature that use energy dissipation have a standard form that can be seen in Equation (2.32).

$$Sh = \alpha\left(\frac{e{d_p}^4}{v^3}\right)^{\beta}Sc^{\gamma} \quad (2.32)$$

Some of the correlations using the energy dissipation approach to mass transfer are listed in Table 2.2 with the experimentally determined constants for α, β and γ. Kawase and Moo-Young (1987) used a combination of the Kolmogoroff theory and the Levich three-zone model to theoretically derive a correlation to determine the liquid-solid mass transfer coefficient. They found the constants α, β and γ to be 0.162, 0.24 and 1/3 respectively. The constants proposed by Kawase and Moo-Young (1987) are preferred because they were derived theoretically, whereas the

other correlations listed in Table 2.2 only fit the constants to their own respective data sets.

Table 2.2: Literature correlations for α, β and γ for use in Equation (2.32)

Reference	α	β	γ	Flow configuration
Sano et al. (1974)	0.4	1/4	-2/3	Stirred tank and bubble column
Deckwer (1980)	0.1	1/4	-1/2	Bubble column
Sanger and Deckwer (1981)	0.545	0.264	-2/3	Bubble column
Asai et al. (1985)	0.31	2/9	-2/3	Packed column

3. Experimental

3.1 Apparatus

3.1.1 Reactor setup

In order to determine the hydrodynamics of the inverse fluidized bed, isothermal experiments were performed using a fluidized bed reactor. The liquid was continuously recycled through the reactor in order to achieve sufficiently high liquid velocities for fluidization and adequate mixing. The feed line was connected to the recycle line in order to feed fresh liquid during the sampling procedure. Fresh feed was required because the volume of the reactor had to be kept constant. A schematic flow diagram of the reactor setup can be seen in Figure 3.1. The middle outlet at the top of the reactor was used to release trapped gas in the reactor and can also be used as a second sampling point. Table 3.1 shows all the equipment used for experiments. Calibration for the feed and recycle pumps can be seen in Appendix A.

Table 3.1: List off all equipment used in experiments and shown in Figure 3.1

Number	Equipment	Description
E-1	CO_2 cylinder	African Oxygen - Technical
E-2	Heat plate	Heidolph Instruments - MR Hei standard
E-3	Reactor vessel	Custom made (Figure 3.2)
E-4	Peristaltic pump	Watson Merlow 520S
E-5	Peristaltic pump	Watson Merlow 520S
E-6	Peristaltic pump	Watson Merlow 323
E-7	Feed tank	
L-1	Gas input line	
L-2	Sample line	
L-3	Gas exit line	
L-4	Recycle line	
L-5	Feed line	
P-1	Pressure regulator	African Oxygen - Afrox Scientific
T-1	Temperature controller	Connected to heat plate - see E-2
V-1	Plug valve	Swagelok - P4T series
V-2	Needle valve	Swagelok - S series

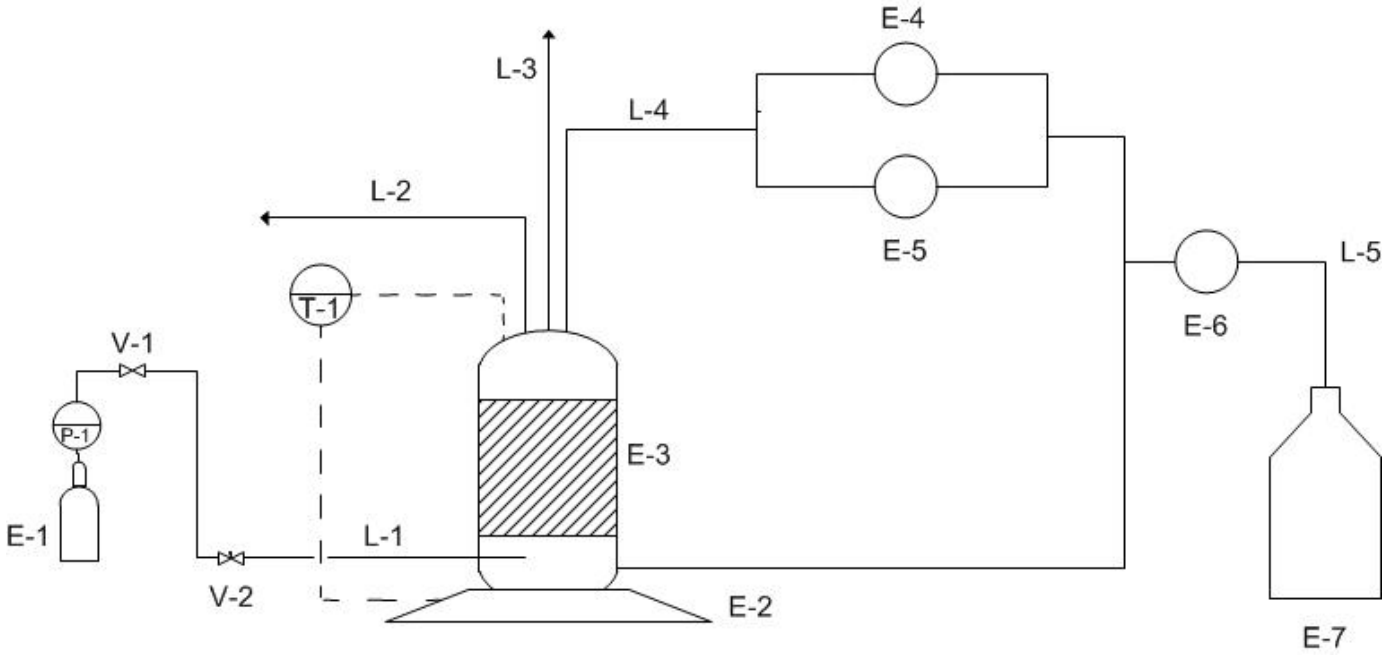

Figure 3.1: A schematic flow diagram of the reactor setup used in all experiments

The reactor vessel used was constructed so that it could be run either up-flow (conventional fluidization) or down-flow (inverse fluidization). Two aluminium liquid distributors were added, one at the top and one at the bottom. An acrylic tube was chosen as the housing of the bed because of its visibility and durability. Four O-rings were added to the top and bottom parts of the reactor to achieve a watertight seal. The temperature was kept at 30 °C (±1 °C) for all the experiments, controlled via the hot plate. A representation of the reactor can be seen in Figure 3.2. Photographs of the reactor dissembled and assembled are shown in Figure 3.3.

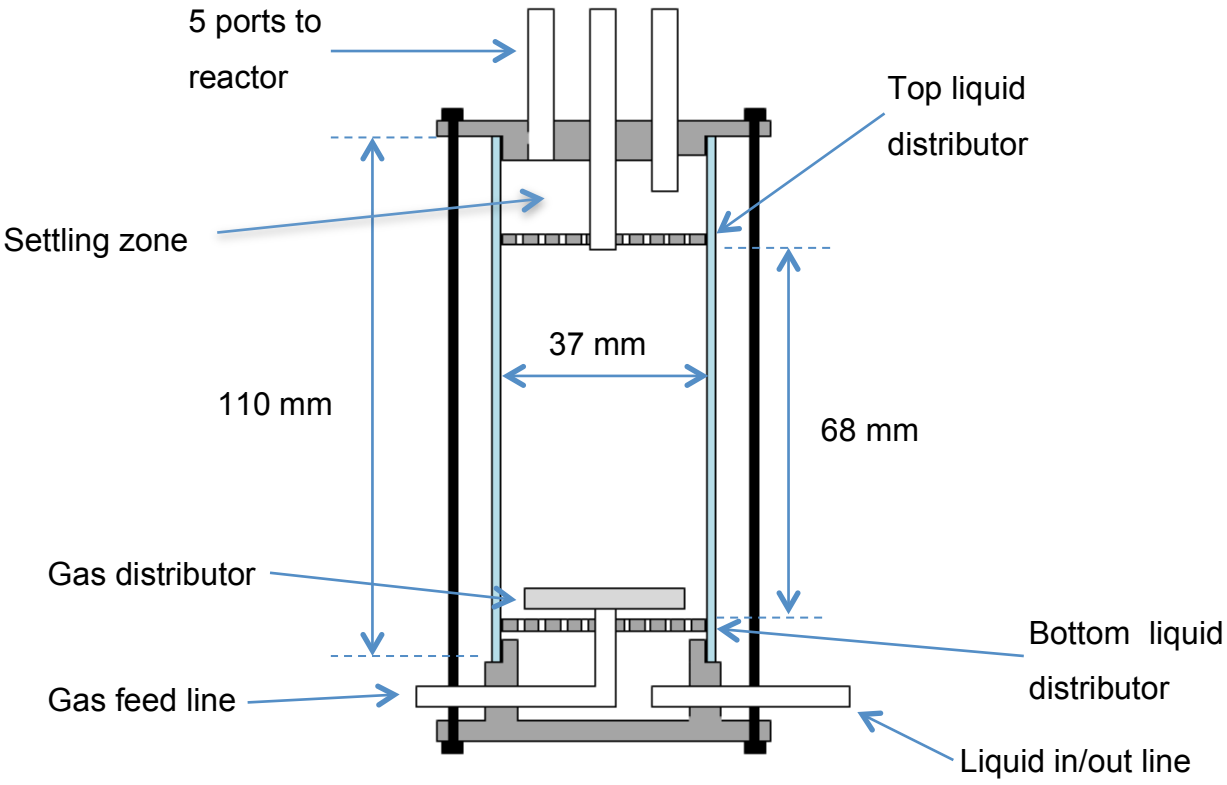

Figure 3.2: Representation of the fluidized bed reactor used in all experiments

a)

b)

Figure 3.3: Photos of the reactor a) assembled and b) disassembled (with two different gas distributor designs)

The reactor can also be run in either liquid-solid or three-phase modes. The detail design of the liquid distributor can be seen in Figure 3.4. For three-phase fluidization only up-flow was possible because counter-current flow with liquid down-flow creates a pressure differential over the top liquid distributer that complicates operation. Photographs of Poraver (low density) and alumina (high density) particles being fluidized can be seen in Figure 3.5.

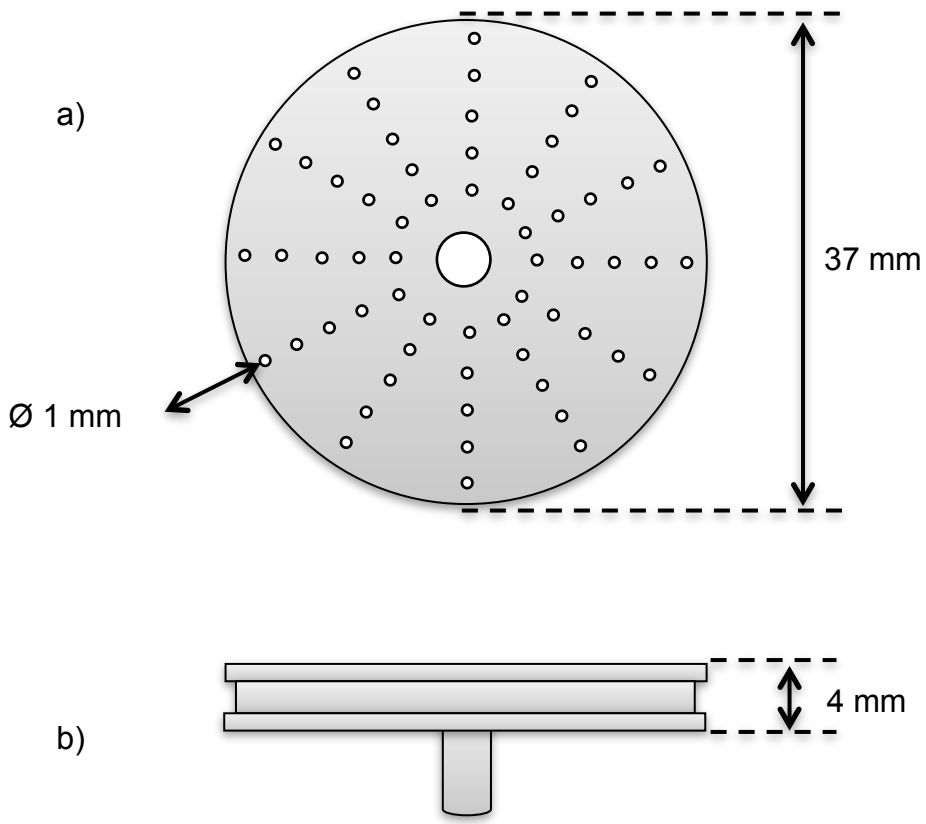

Figure 3.4: Liquid distributer design: a) top view b) side view

Two different gas distributors were designed to introduce gas at the bottom of the reactor for three-phase fluidization. The gas distributor is screwed into place right above the bottom liquid distributor. Two designs were made in order to determine whether the design makes a difference to the experimental results. The two designs can be seen in Figure 3.6. The gas flow rate used in this study was low enough so that there was no difference between the two designs. The distributer shown in Figure 3.6 (a) was used for all further experiments. An expanded view of the distributor design can be seen in Appendix C.

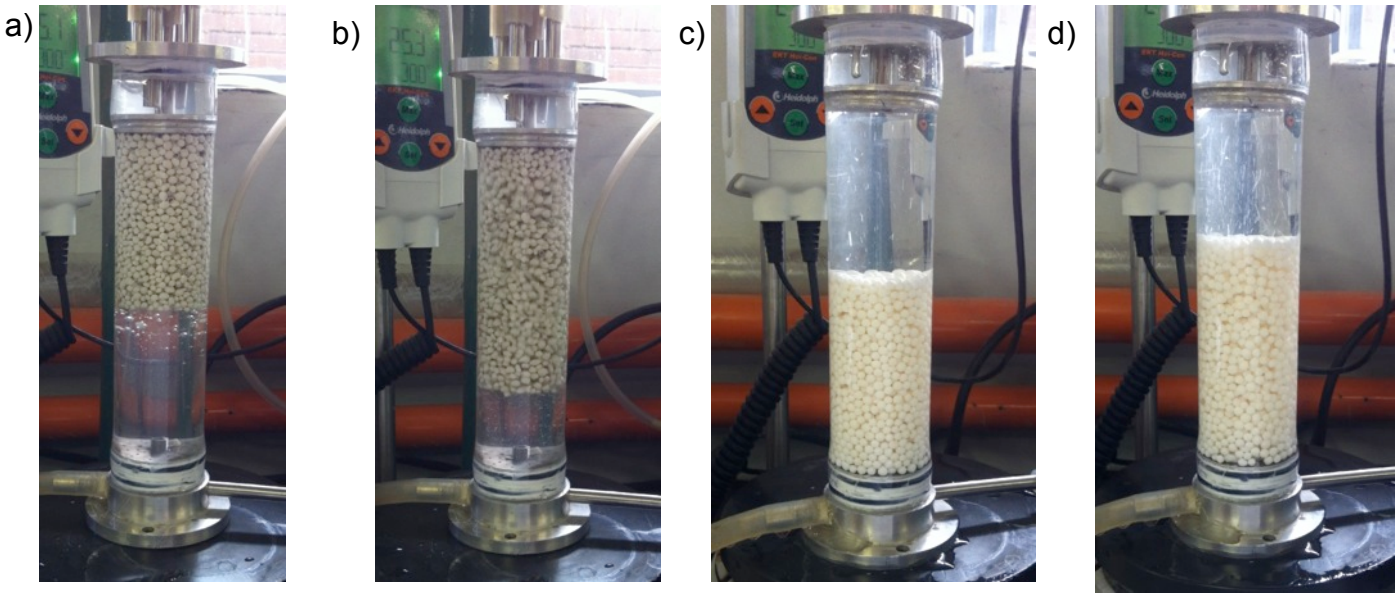

Figure 3.5: a) Poraver particles u_l = 0 m/s b) Poraver being fluidized in liquid-down flow mode u_l = 0.039 m/s c) alumina particles u_l = 0 m/s d) alumina being fluidized in liquid up-flow mode u_l = 0.039 m/s

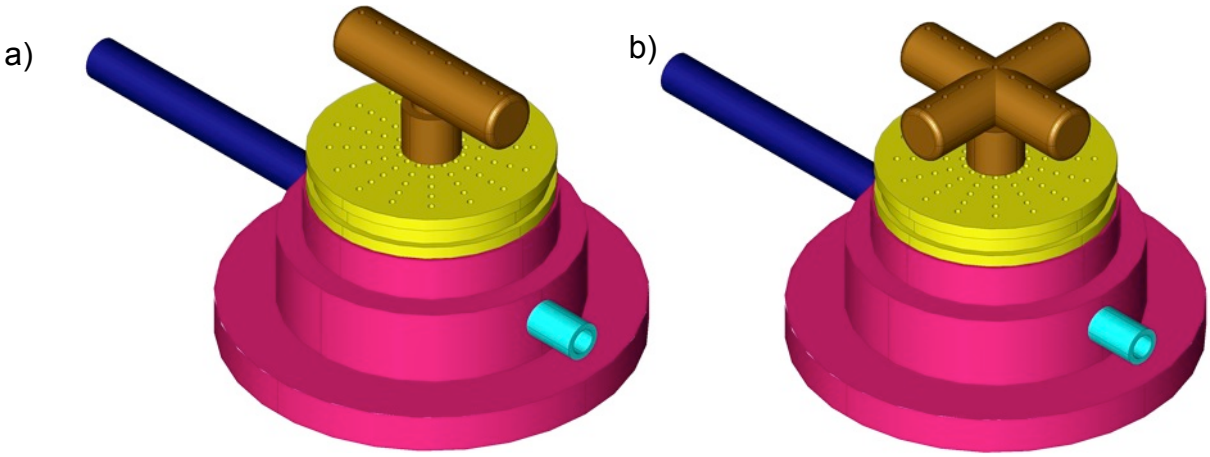

Figure 3.6: Drawing of the bottom half of the inverse fluidized bed, where the yellow part is the liquid distributor and the bronze part is the gas distributor. (a) and (b) represent the two different designs

3.2 Particles

3.2.1 Types

In the experiments performed, four different particles were fluidized. The particles were chosen with different particle densities in order to determine liquid-solid mass transfer dependencies on density difference between the particle and the liquid employed. The four particles chosen were aluminium oxide (alumina), Poraver (expanded glass), polypropylene (PP) and polyoxymethylene (POM). These particles are summarized in Table 3.2.

Table 3.2: Different particles used in this study

Type	Mean diameter (mm)	Diameter variance (%)	Sphericity	Density (g/l)
POM	3.85	0.5	1	1 580
Alumina	3.5	8	0.99	2 300
Poraver	3	33	0.9	320
PP	2	10	0.98	855

Poraver is a very porous particle, therefore the dry density shown in Table 3.2 is not a true representation of the particle density in the reactor. When porous particles are submerged in liquid, the liquid displaces the trapped air and therefore changes the density. The wet particle density is a better representation. Poraver particles were submerged in distilled water and weighed at different time intervals in order to observe the density variation with time. The results can be seen in Figure 3.7. It can be seen that the density reaches 550 g/l within 3 minutes. After saturation the density then stays fairly constant around 590 g/l. This density was used in all hydrodynamic correlations for Poraver particles.

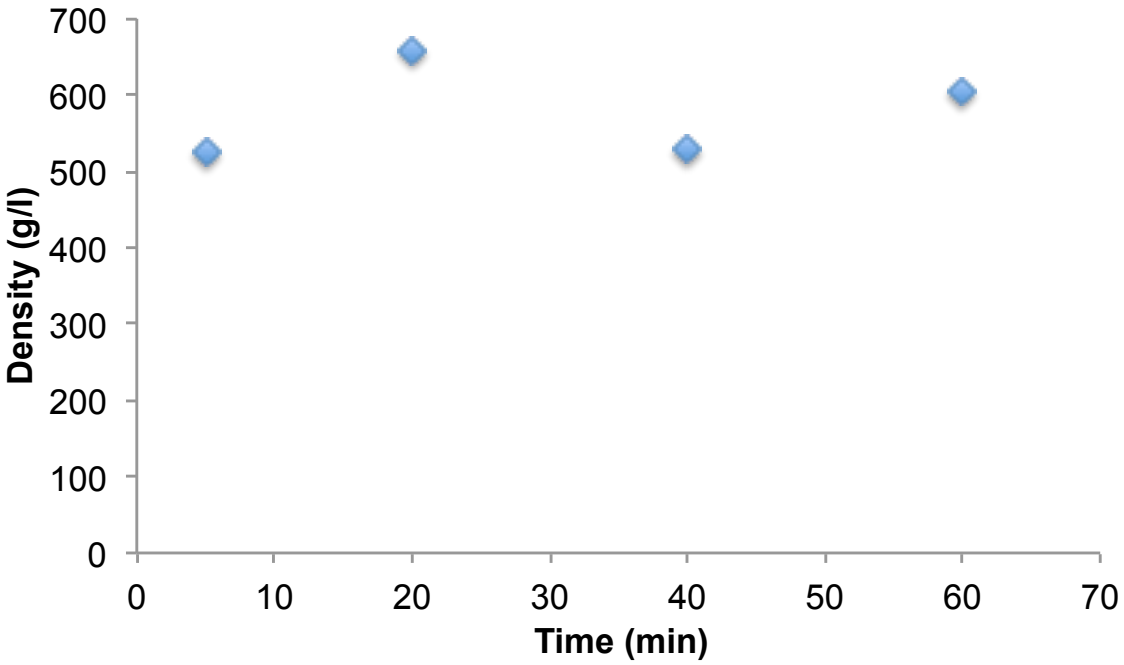

Figure 3.7: Particle density of Poraver particles measured with different submersion times in water

3.2.2 Particle preparation

The benzoic acid dissolution method developed by Gamson (1951) was chosen for the liquid-solid mass transfer experiments. Shen, Geankoplis and Brodkey (1985) and Arters and Fan (1990) used a modified version of the method of Gamson (1951). In the previously mentioned work the authors used pelletized benzoic acid particles for their experiments with good results. This method was modified in order to use different types of particles. For this study the benzoic acid was coated onto the different particles studied. The different types of particles and the amount of benzoic acid added are shown in Table 3.3.

The benzoic acid was brought to its melting point (124 ^{o}C) in an oven until it was all melted. The particles were placed in a mesh basket, which in turn was placed in a beaker. Some of the particles have a lower melting point than benzoic acid, therefore the particles were kept at a low temperature (20 ^{o}C). This ensured sufficient coating without any particle deformation. The POM particle surfaces were roughened with

sandpaper to ensure proper adhesion of the benzoic acid. The results of the coating procedure can be seen in Table 3.3.

Table 3.3: Different particles coated with the amount of benzoic acid (BA) added

Type	Diameter (mm)	BA (x10^3 g) coated per particle	Number of particles used per experiment	Total external area of particles (x10^{3}m^3)	Total mass BA added (g) per experiment
Alumina	3.5	10.42	33	1.269	0.344
Poraver	3	3.79	44	1.244	0.167
PP	2.4	5.24	70	1.267	0.367
POM	3.85	25.75	27	1.257	0.695

3.3 Data interpretation

The boundary layer theory is used to describe the liquid solid mass transfer. It is based on a stagnant film of fluid that is formed around the particle. Because of the stagnant film of fluid that is formed around a catalyst pellet diffusion through this stagnant film is needed. The bulk concentration of a species will not be the concentration that the active site on the catalyst surface will see. If it is assumed that the properties like temperature and concentration at the edge of the film are the same as the bulk fluid of thickness δ, then the flux through the film can be described by the following equation (Fogler, 2009:773):

$$W_A = \frac{D_{AB}}{\delta} . [C_{Ab} - C_{As}] \tag{3.1}$$

Where C_{Ab} and C_{As} are the concentrations of species A in the bulk and surface respectively. The ratio between the diffusivity D_{AB} to the thickness of the film δ is called the mass transfer coefficient, k_c. Then the reaction rate due to mass transfer becomes:

$$r_{a\backslash MT} = k_{cA} . [C_{Ab} - C_{As}] \tag{3.2}$$

In order to determine the mass transfer coefficient from the dissolution method, the reaction rate is written in terms of reactor volume to give Equation (3.3).

$$\frac{dC_{Ab}}{dt} = \frac{k_s a_s .[C_{sat} - C_{Ab}]}{V} \quad (3.3)$$

Where

a_s is the total external area of the coated particles,

V is the reactor volume,

C_{Ab} is the concentration of benzoic acid in the bulk fluid and

C_{sat} is the saturation concentration of benzoic acid.

The saturation concentration of benzoic acid in water was experimentally determined at 30 ^{o}C to be 5.64 g/l. The result obtained compares well with the values obtained by Delgado (2006) and Qing-Zhu et al. (2006). For all the experiments the area of the particles was kept the same in order to compare results (see Table 3.3).

Since the thickness of the benzoic acid layer varied substantially, the dissolution experiments resulted in partial depletion of benzoic acid on sections of the particle surface. To ensure proper quantification of the specific mass transfer coefficient, only the initial dissolution data were considered where the particles are still fully covered by benzoic acid. This can be seen in Figure 3.8. The model prediction continues until saturation is reached. In the experiments this saturation concentration was never reached because only a limited amount of benzoic acid is available to dissolve.

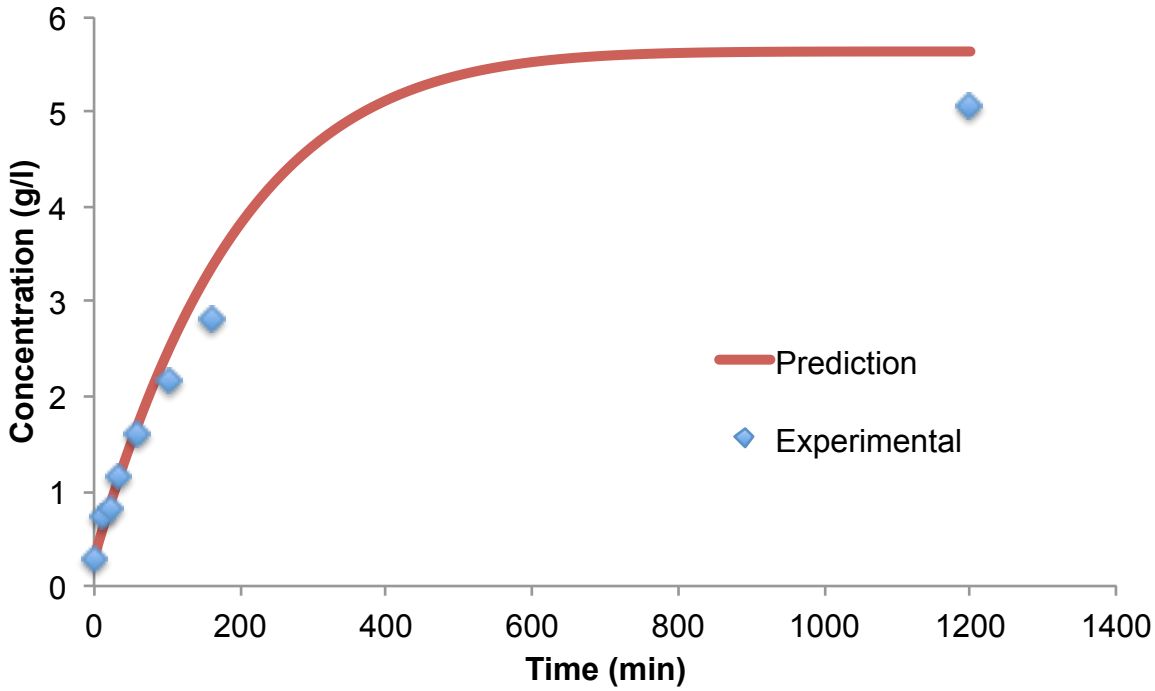

Figure 3.8: Concentration of benzoic acid in a stagnant beaker setup against time for coated polypropylene particles

A model was correlated to determine the concentration at which partial coverage occurs. For each particle type a different amount of benzoic acid is loaded into the reactor because of density and diameter differences. This in turn influences the maximum concentration (C_{max}) possible inside the reactor. For all the particles, runs were done in a stagnant beaker in order to more accurately determine when partial coverage occurs (C_{PC}). For the beaker runs, the same volume of water was used as the reactor vessel volume, and the same amount of particles were loaded that were used in the fluidization runs. This was done in order to keep the concentrations determined useable for the fluidization runs. The concentration at which the data and the prediction had an error of more than 10% was taken as the concentration at which partial coverage occurs. Table 3.4 shows these two concentrations for each particle type. Experimental fits were only done until C_{PC} was reached to quantify only liquid-solid mass transfer.

Table 3.4: Fit criteria for the four particle types. Partial coverage occurs at C_{PC}

Type	Total mass BA added (g) per experiment	C_{max} (g/l)	C_{PC} (g/l)
Alumina	0.344	4.702	1.494
Poraver	0.167	2.281	0.725
PP	0.367	5.017	1.594
POM	0.695	5.64	3.022

In the fluidization setup sampling volumes were not insignificant and had to be refilled with water. This causes step changes in the benzoic acid concentration in the vessel at the times when samples are drawn and replaced with pure water. The model was adapted and a new integration was done after each data point (time of sampling). The sampling size is known; therefore this step integration was used to determine all liquid-solid mass transfer coefficients. For data representation purposes, however, Equation (3.3) can be adapted to give a smooth prediction with inclusion of the step sampling. The model used can be seen in Equation (3.4), where V_{samp} is the volume of liquid taken out of the reactor due to sampling per minute. This simulates a very small concentration change each minute, which adds up to the total volume of all the samples drawn during each run. Figure 3.9 shows the resulting prediction along with a smooth prediction. The smooth prediction is used in all further data interpretations for ease of visualization.

$$\frac{dC_{Ab}}{dt} = \frac{k_s a_s .[C_{sat} - C_{Ab}]}{V} - \frac{C_{Ab}.[1-(V-V_{samp})]}{V} \tag{3.4}$$

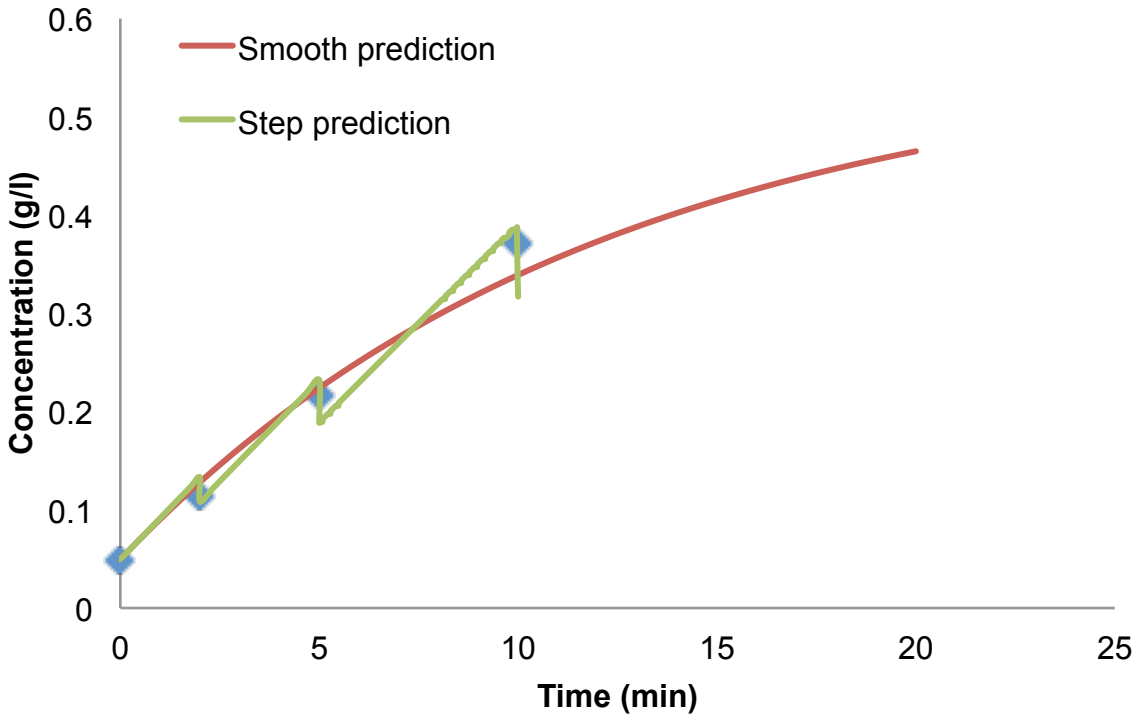

Figure 3.9: Comparison between a true step prediction and an adapted smooth prediction for the fluidization of polypropylene at a liquid velocity of 10.5 mm/s

4. Results and discussions

4.1 Repeatability

The reactor design allowed for samples to be taken at two different places in the reactor. Repeat runs were done in order to determine the best sampling position. It was found that repeatable results were obtained if the samples were taken in the settling zone above the top liquid distributor (see Figure 3.2). In order to develop and perfect the dissolution method in terms of sampling method, coating procedure and sampling period, experimental runs were done on different beaker reactor setups. These results can be seen in Appendix B.

Table 4.1 shows all the runs on which repeat runs were performed, along with the error between the original and repeat runs. Figures 4.1 and 4.2 are examples of four repeat runs done on two different particles, Poraver and polypropylene. The AARE values were determined by comparing the fitted liquid-solid mass transfer coefficients for the repeat runs to the originally fitted mass transfer coefficients. The AARE between all the repeat runs was 4%, while the maximum error was 9.52%. From these data it was concluded that the reactor setup and sampling method gives repeatable results.

Table 4.1: The AARE of liquid-solid mass transfer coefficient for repeat runs

Particle type	U_l (mm/s)	Flow direction	Error for repeat run
PP	17.3	Down	5%
PP	38.6	Down	5.60%
PP	17.53	Up	9.52%
Poraver	29.8	Down	1%
Poraver	38.6	Down	1.50%
Poraver	17.53	Up	0.50%
POM	28.05	UP	2.38%
Alumina	50.9	Up	8.79%
Alumina	34.19	Up	2.04%

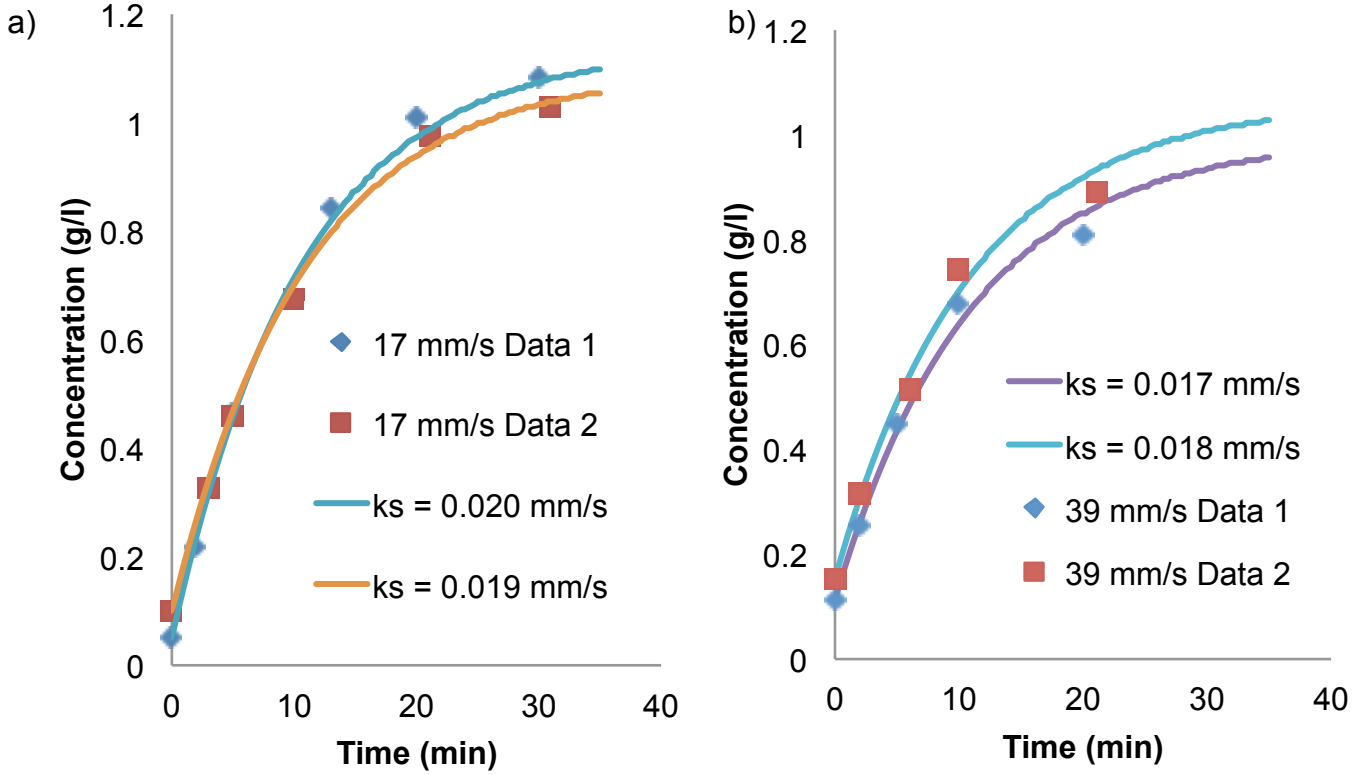

Figure 4.1: a) Two identical runs done in a packed bed with polypropylene particles (u_l = 17 mm/s). b) Two identical runs done in a packed bed with polypropylene particles(u_l = 39 mm/s)

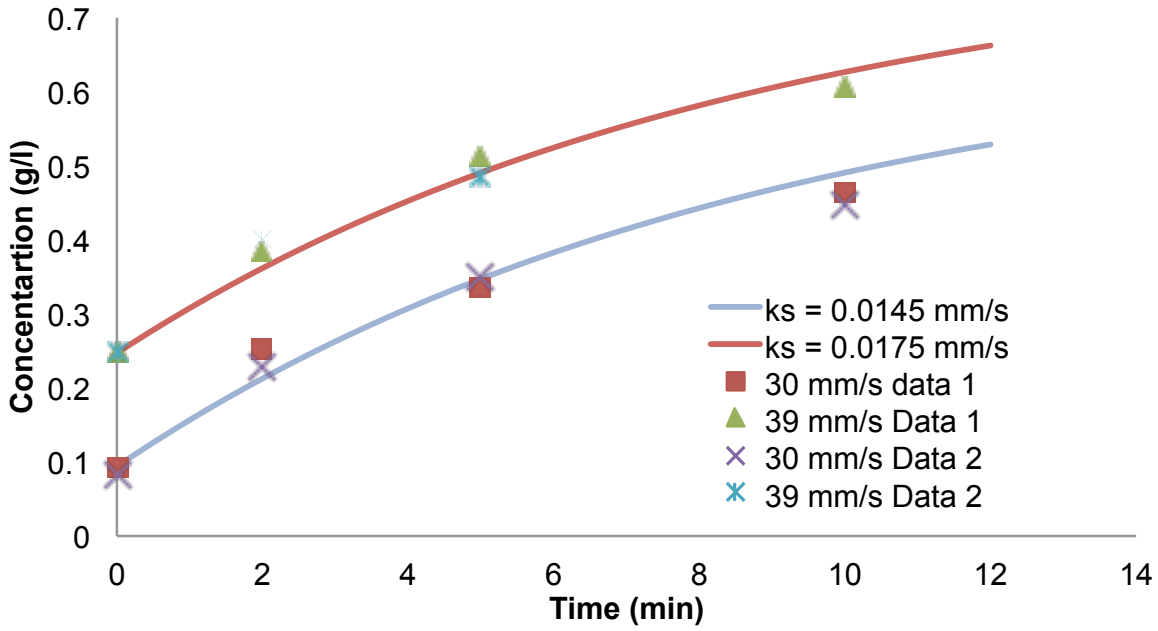

Figure 4.2: Two identical runs at u_l = 30 mm/s and two at u_l = 39 mm/s done in a fluidized bed with Poraver particles

4.1.1 Influence of reactor length

The effect of bed height on mass transfer was investigated. A longer reactor bed was constructed and repeatability runs were done. The reactor length was doubled to 150 mm and the unexpanded particle bed was doubled to 80 mm.

The reactor was run in down-flow mode for fluidization, and the results can be seen in Figure 4.3. As expected, the liquid-solid mass transfer remained unchanged. The deviation between the two fitted k_s values was found to be 3.45 %, which is within experimental error. This indicates that neither the reactor length nor the particle bed height has any influence on the liquid-solid mass transfer.

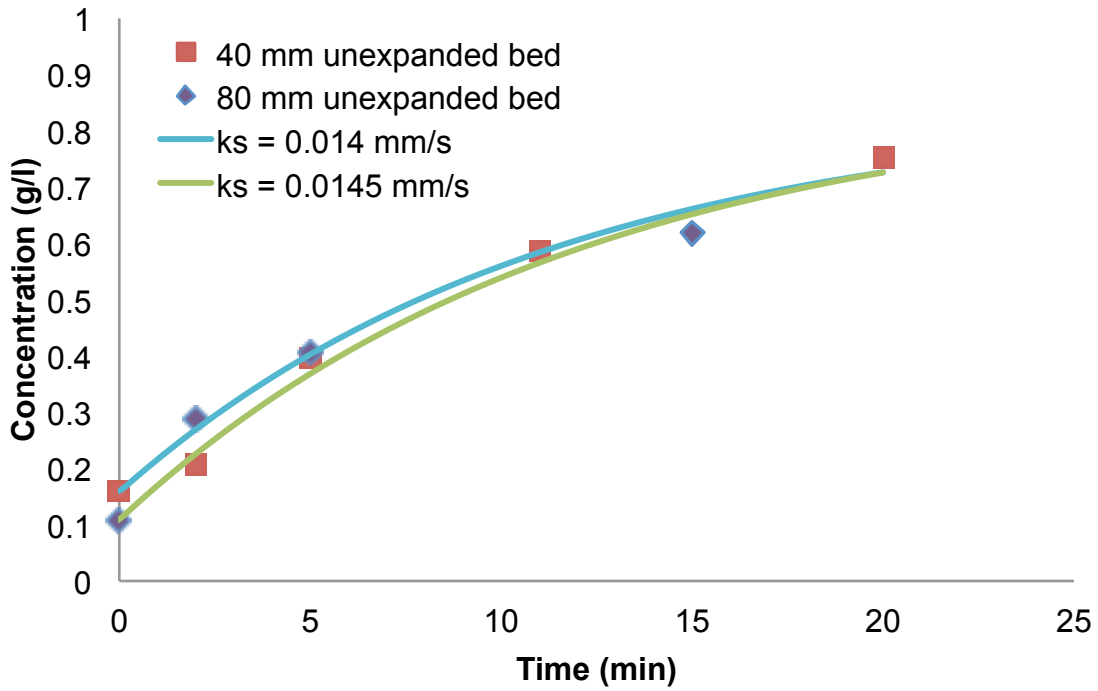

Figure 4.3: Fluidized runs with polypropylene at a superficial liquid velocity of 26 mm/s

4.2 Two-phase liquid-solid mass transfer

4.2.1 Fluidized bed

In order to determine the liquid-solid mass transfer coefficient, different runs were done at different liquid velocities. Figure 4.4 shows the dissolution runs for three different liquid velocities in an inverse fluidized bed with polypropylene particles.

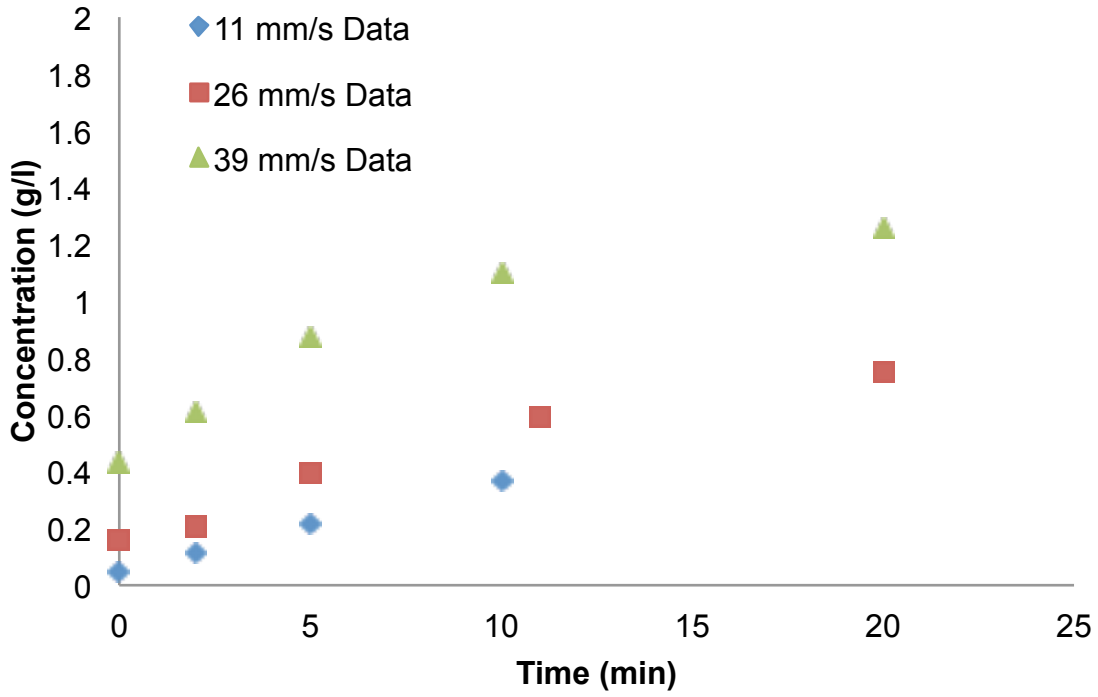

Figure 4.4: Dissolution runs done with polypropylene at different superficial liquid velocities

The difference in initial concentrations is due to the fact that the reactor is operated for a few minutes before the first sample can be taken. This needs to be done to remove gas bubbles from the reactor. The first sample was always taken as tine zero. This does not influence the k_{ls} analysis as long as C_{PC} is not attained during start-up.

Numerous trends similar to those in Figure 4.4 were generated for the different particle types in both up-flow and down-flow modes. These trends were used to obtain a liquid-solid mass transfer coefficient for each run. These mass transfer coefficients could then be compared with each other and with correlations found in

the literature. The results of the fluidization runs for the four particles can be seen in Figure 4.5.

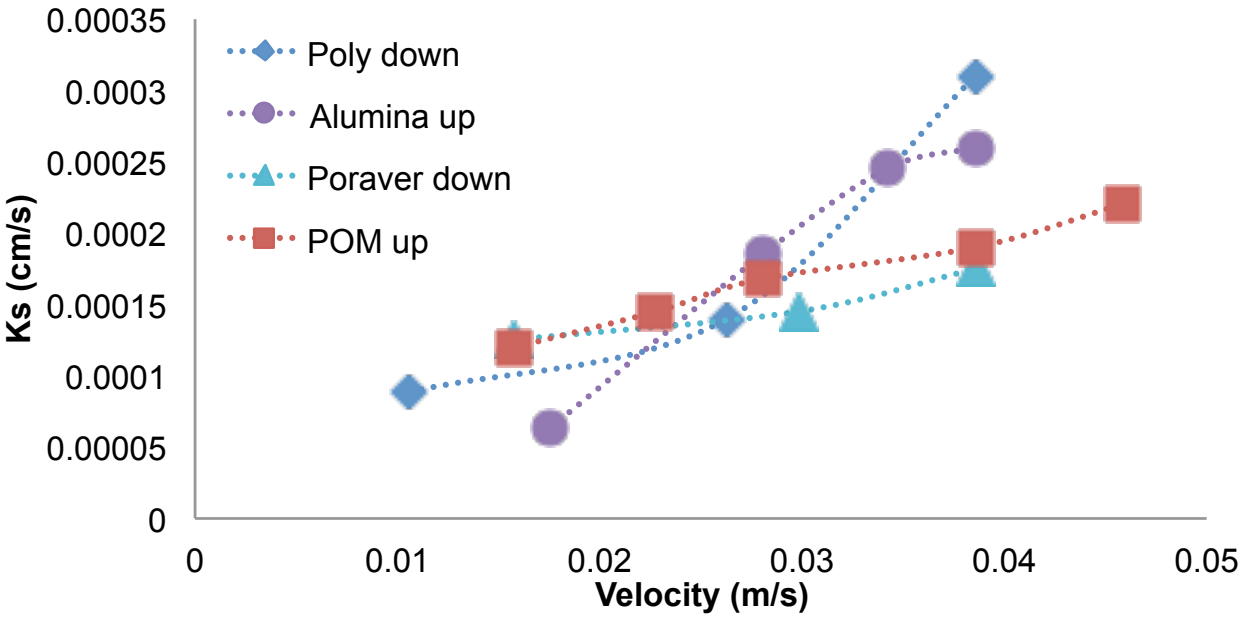

Figure 4.5: Liquid-solid mass transfer as a function of superficial liquid velocity for fluidization runs

It is seen in previous studies that the liquid-solid mass transfer coefficient increases when approaching minimum fluidization velocity (Nikov and Delmas, 1987) and remains fairly constant after minimum fluidization velocities have been achieved (Hassanien et al., 1984; Arters and Fan, 1986; Prakash et al., 1987). All the correlations found in the literature are only applicable in the smooth fluidization regime. The question arises whether there exists a higher quantifiable velocity where a regime change might occur. For gas-solid fluidization there exists a velocity (u_c) where the bed enters the turbulent regime. It had to be tested whether u_c can effectively be applied to liquid-solid fluidization. Minimum fluidization velocities and onset of turbulent velocities were calculated for the particles used in this study.

For minimum fluidization velocities, Renganathan and Krishnaiah (2003) found that the equation proposed by Wen and Yu (1966) gives satisfactory results when applied to inverse liquid-solid fluidization. In order to calculate u_c, however, different correlations were assessed. In previous studies only heavy particles were

investigated and therefore the turbulent regime was difficult to attain and was not investigated for liquid-solid fluidization. Correlations found in the literature are based on gas-solid systems (with some liquid-solid data) and were tested to see if they predict proper u_c values for the data obtained in this study. The correlation proposed by Nakajima et al. (1991) was used for Poraver, POM and polypropylene because it can be used for a very wide variety of particles. Their correlation can be seen in Equation (4.1):

$$Re_c = 0.633Ar^{0.467} \tag{4.1}$$

The correlation proposed by Lee and Kim (1990) was chosen for alumina because their study was done with glass beads with similar physical characteristics to those of alumina. The authors, however, used air as their fluidization medium. Their correlation can be seen in Equation 4.2:

$$Re_c = 0.7Ar^{0.485} \tag{4.2}$$

From these Re_c values the onset of turbulence velocities (u_c) can be determined. When these flow regimes were added to the experimental data different trends were identified with more ease, as seen in Figure 4.6. Nikov and Delmas (1987) also found that the mass transfer rate increases near minimum fluidization velocities as seen for alumina and POM particles. Hassanien et al. (1984), Arters and Fan (1986) and Prakash et al. (1987) all found that when the minimum fluidization velocity is reached the mass transfer stays fairly unchanged. This trend can be seen in Figure 4.6 for all four particles tested.

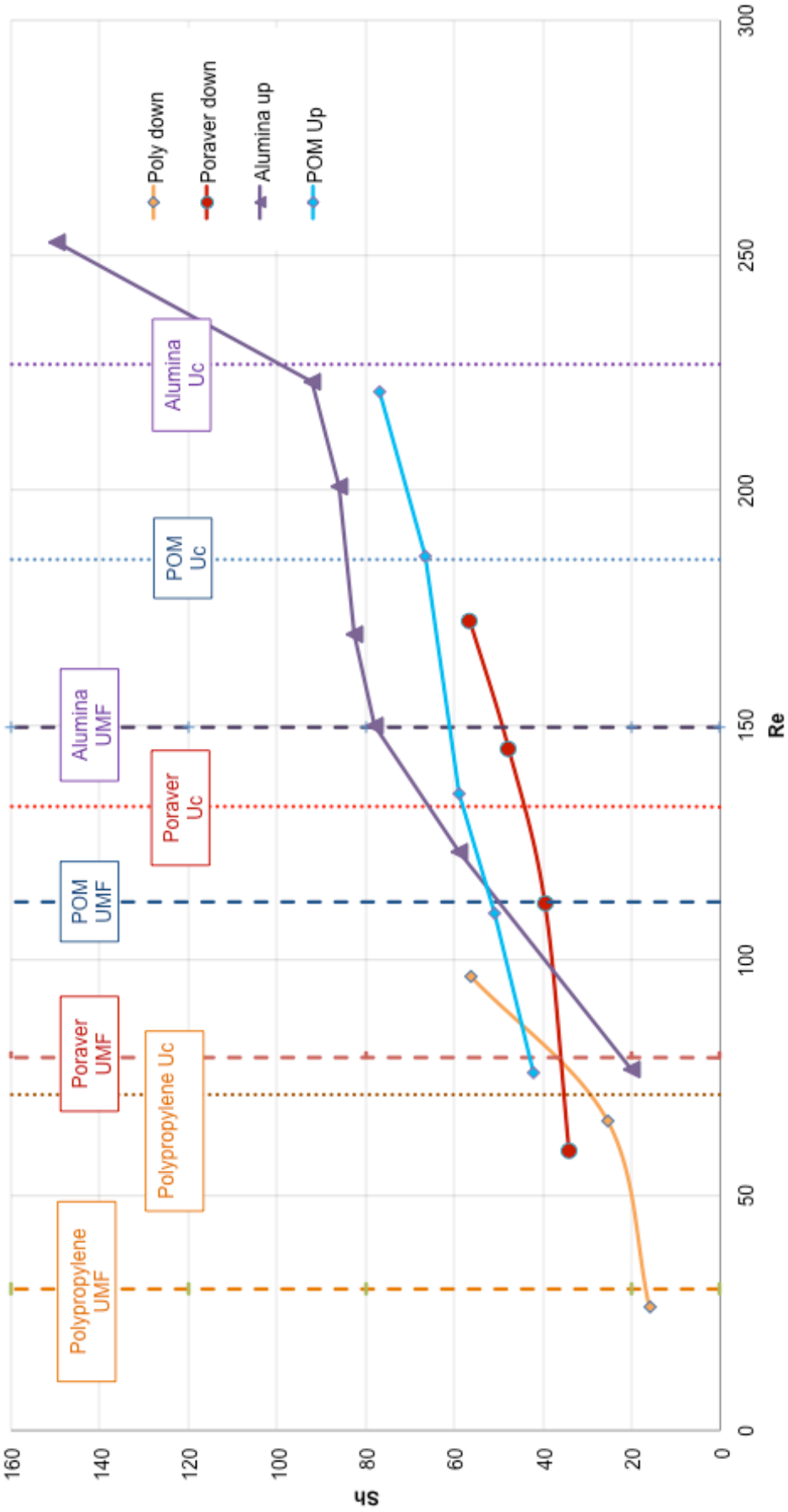

Figure 4.6: Experimental results found with indication of critical liquid superficial velocities

It can be seen in Figure 4.6 that the Sh number increases with an increase in Re for all four particles. It is also seen that higher Sh values are possible for particles with higher minimum fluidization velocities. The liquid-solid mass transfer increases until u_{mf} is reached. For particles with higher u_{mf} values, higher mass transfer coefficients are possible. When the liquid velocity exceeds that of u_c a slight increase in mass transfer coefficients was seen for POM and Poraver, whereas for PP and alumina a greater increase was seen. The greater increase for alumina can be due to the fact that alumina particles are very heavy and with increased liquid velocities the collisions between the particles may have caused some coated benzoic acid to be chipped off the particles. Polypropylene has the smallest density difference and therefore at very high liquid velocities the particle bed expanded the full length of the reactor causing collisions between the particles and the liquid distributor. No decisive conclusions can be reached on this increase after u_c because it only occurs for two of the four particles. Table 4.2 shows the density differences between the four particles and water along with the Reynolds number at minimum fluidization and u_c. This gives an indication where the $u_{mf} – u_c$ window is reached.

Table 4.2: Density differences and Reynolds numbers at u_{mf} and u_c

Particle type	$\Delta\rho$ (kg/m^3)	Re_{mf}	Re_c
Polypropylene	- 145	30.1	71
Poraver	- 410	79.3	133
POM	+ 580	112.4	185
Alumina	+ 1300	149.6	227

A number of correlations found in the literature to predict the liquid-solid mass transfer were tested, but the correlation proposed by Kawase and Moo-Young (1987) (Equation (2.32)) was found to fit the data the best. The Poraver particles are not totally spherical and the correlation had to be adapted to take this factor into account. Arters et al. (1988) suggested adding the term $\phi^{0.6}$ for non-spherical particles. The correlation proposed by Kawase and Moo-Young (1987) with the sphericity adaptation was compared to all the experimental data; the results can be seen in Figure 4.7. Sphericity values can be seen in Table 3.2.

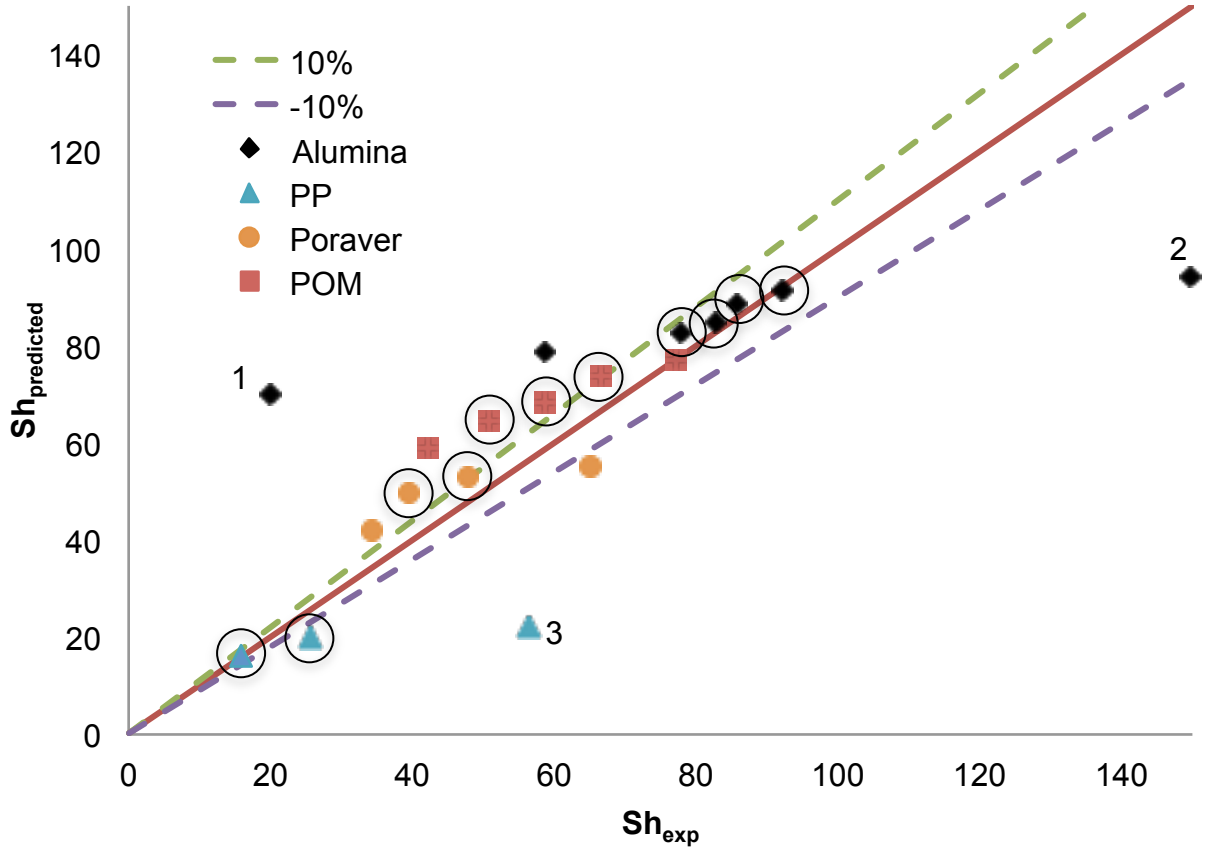

Figure 4.7: Comparison between experimental data and the correlation proposed by Kawase & Moo-Young (1987). The circled data points fall in the u_{mf} – u_c window

It can be seen from Figure 4.7 that the correlation proposed by Kawase and Moo-Young (1987) effectively fits the experimental data from the minimum fluidization velocity until the onset of turbulent velocity. When all the data points for all four particles were compared with the correlation of Kawase and Moo-Young (1987), however, an AARE of only 30.7% was achieved. The first data point for alumina (1 in Figure 4.7), however, can be left out because the superficial velocity is such that the bed is still packed and cannot be predicted with a fluidized bed correlation. The last data points for polypropylene (PP) (3 in Figure 4.7) and alumina (2 in Figure 4.7) can also be left out of the correlation comparison because those two points exhibited a huge increase in Sh, and it is unclear if a new regime was entered (as discussed earlier). When these three data points are left out, the Kawase and Moo-Young (1987) model gives an AARE of 18%.

The correlation proposed by Kawase & Moo-Young (1987) can be seen below:

$$Sh = 0.162\left(\frac{e{d_p}^4}{v^3}\right)^{0.24} Sc^{1/3} \quad (2.32)$$

The minimum fluidization velocity plays a big role and therefore a new model was correlated that includes the particle characteristics in the form of the dimensionless group, the Archimedes number. The correlation proposed can be seen in Equation (4.3).

$$Sh = 0.05 Re^{0.42} Sc^{0.66} |Ar|^{0.17} \quad (4.3)$$

The addition of the Archimedes number makes for a more universal and robust correlation. Adding the particle characteristics to the correlation makes the correlation more mechanically sound. The values for the constants were determined by comparing the correlation to the experimental results and minimizing the AARE The absolute value of the Archimedes number needs to be taken into account because some of the particles have lower densities than that of water and therefore yield a negative Archimedes number. Equation (4.3) gave an AARE of 8% when compared to the experimental results (excluding the three previously mentioned data points), which is an improvement on the correlations found in the literature. This correlation can be used for different particle densities up to the onset of turbulent regime velocity (u_c). Figure 4.8 shows how the new correlation compares to the experimentally determined Sh numbers (Sh_{exp}).

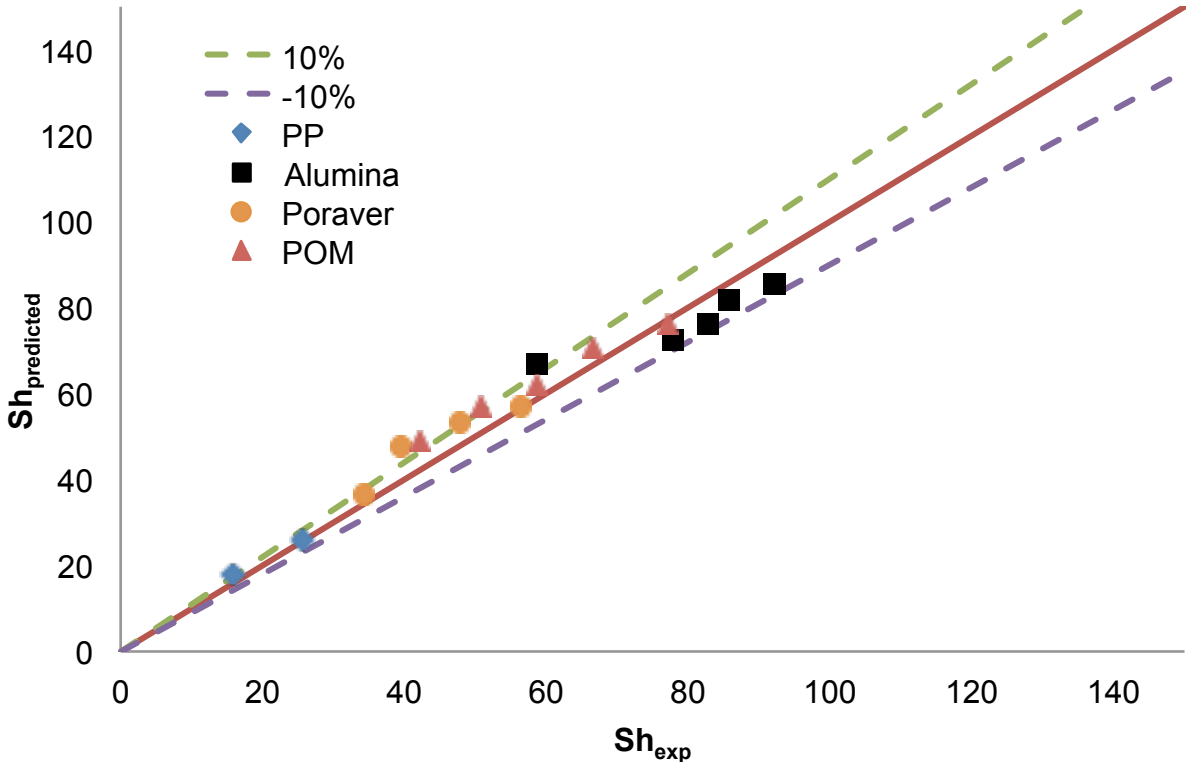

Figure 4.8: Comparison between the new correlated model (Equation 4.3) and the experimental results

The Reynolds number has the biggest influence on the Sherwood number (or energy dissipation), where the superficial liquid velocity determines Sh. For particles with higher densities, higher superficial liquid velocities are needed to reach the minimum fluidization velocity. The Schmidt number is still included in the correlation to incorporate the diffusion constant.

Density difference (Δρ) has the biggest influence on u_{mf} and is therefore a big driving force in achieving higher liquid-solid mass transfer rates. For higher Δρ, higher mass transfer coefficients are achieved. With the inclusion of the Archimedes number (with a reasonably small power) in the correlation, the density difference factor is included in the prediction of liquid-solid mass transfer rates. This helps improve the liquid-solid mass transfer correlation.

There seems to be no influence when conventional fluidization is compared to inverse fluidization. Poraver and POM have similar Δρ values except for the direction of fluidization, and it is seen that their mass-transfer coefficients are virtually the

same. POM only slightly outperforms Poraver because its Δρ is slightly higher. It can be concluded from the presented results that the direction of liquid flow has no influence on liquid-solid mass transfer for two-phase fluidized beds.

4.2.2 Packed bed

All four particle types can also be run in a packed bed mode. For the alumina and POM particles the reactor was run in a down-flow manner while for the Poraver and polypropylene particles the reactor was run in an up-flow manner. Similar dissolution trends were found to the ones shown in the previous section, and liquid-solid mass transfer coefficients were determined from those trends.

These data were compared to one of the correlations found in the literature to see how it compares to previous studies. The most extensively used model in the literature is the one by Thoenes and Kramers (1958). The authors tested eight different particles in a packed bed manner and compiled a model to fit these data and those of previous studies. They correlated different complex correlations but found that the correlation seen in Equation (4.4) gave a deviation of only ±10% for all 438 mass transfer rates. This correlation was compared to the data obtained. Figure 4.9 shows the data for two of the particle types used compared to the Thoenes and Kramers (1958) model.

$$Sh' = 1.0\ (Re')^{\frac{1}{2}} Sc^{\frac{1}{3}} \tag{4.4}$$

Sh' and Re' are defined in Equations (4.5) and (4.6), where Φ is the void fraction of the packed bed and γ is the external shape factor.

$$Sh' = \frac{Sh\,\Phi}{(1-\Phi)\gamma} \tag{4.5}$$

$$Re' = \frac{Re\,\Phi}{(1-\Phi)\gamma} \tag{4.6}$$

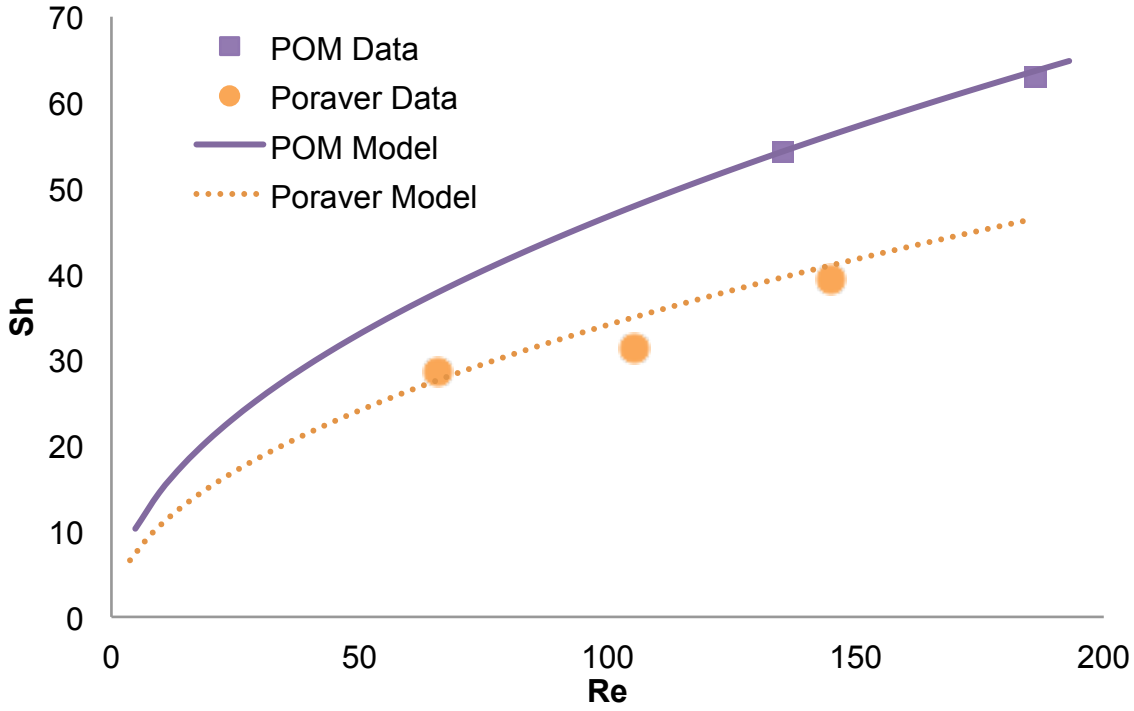

Figure 4.9: Thoenes and Kramers (1958) model compared to data obtained in the packed bed setup for POM and Poraver

It is seen from Figure 4.9 that the correlation predicts the data obtained within the 10% error claimed by Thoenes and Kramers (1958). The reason for the different trends predicted is attributed to the void fraction differences between the two particle types. The void fraction is included in the correlation by Thoenes and Kramers (1958) as seen in Equations (4.5) and (4.6). These results indicate that the data obtained are accurate and can be compared with confidence.

The model proposed by Thoenes and Kramers (1959) was compared with the model correlated for a fluidized bed in Equation (4.3). These are both explicit equations and can be mathematically compared in order to see the performance differences between packed beds and fluidized beds. Figure 10 shows the Sherwood ratio where Sh_{PB} is the Sherwood number for a packed bed and Sh_{FB} is the Sherwood number for a fluidized bed. Where the ratio is higher than 1, the fluidized bed outperforms the packed bed when liquid-solid mass transfer is compared. A constant void fraction was used for all the particles compared in the packed bed setup.

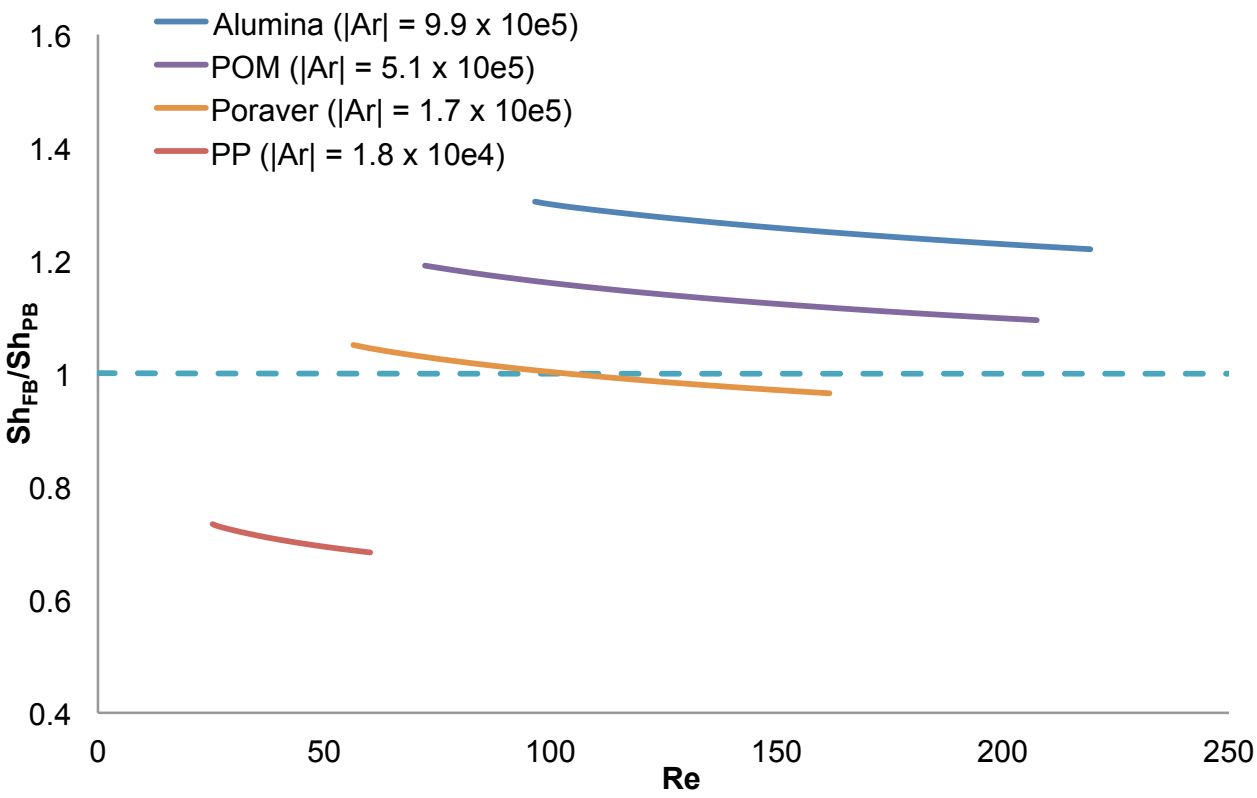

Figure 4.10: Comparison between packed bed performance and fluidized bed performance for different Re and Ar values

The comparison between the two correlations, for a change I mass transfer with a change in liquid velocity, could only be done between u_{mf} and u_c for each particle type, because the fluidized bed model is only valid for this window. From Figure 4.10 it can be seen that the Sherwood ratio is fairly independent of the liquid velocity. The Archimedes number, which is driven by the density difference, has the biggest influence on the Sherwood ratio. For high Ar values (like with alumina) the fluidized bed outperforms the packed bed by far.

It is interesting to note that when the density difference becomes smaller, the fluidized bed only slightly outperforms the packed bed setup. For the Poraver particles, $\Delta\rho$ = -410 kg/m^3, the mass transfer rates are fairly similar for packed beds and fluidized beds. Poraver is on the boundary between fluidized bed and packed bed. For low liquid velocities the fluidized bed performance is better, whereas for high liquid velocities the packed bed setup has the best performance.

From the Polypropylene runs it can be seen that the liquid-solid mass transfer for the packed beds is better than for the fluidized beds. The very small density difference ($\Delta\rho$ = -145 kg/m^3) influences the liquid-solid mass transfer to the extent that the packed bed substantially outperforms the fluidized bed.

4.3 Three phase fluidization

In order to investigate the influence of three-phase fluidization on the liquid-solid mass transfer, gas was introduced at the bottom of the reactor co-current to the liquid flow. For three phase fluidization only up-flow could be compared because counter-current flow with liquid down-flow creates a pressure differential over the top liquid distributer that complicates operation. For this reason only the two higher-density particle types, POM and alumina, were tested in three-phase (up-flow) fluidization. For future development a different reactor design will be needed in order to eliminate the differential pressure. A reactor is needed where the liquid can be introduced at the side of the reactor with a gas-settling zone at the top.

A number of runs were done at different liquid velocities. A constant gas vvm (volume of gas fed to the reactor per volume of the reactor) of 162 ml/ml.min was fed to the reactor for all runs. The results obtained for alumina particles can be seen in Figure 4.11. The minimum fluidization velocities can be determined using the correlations in Section 1.4.

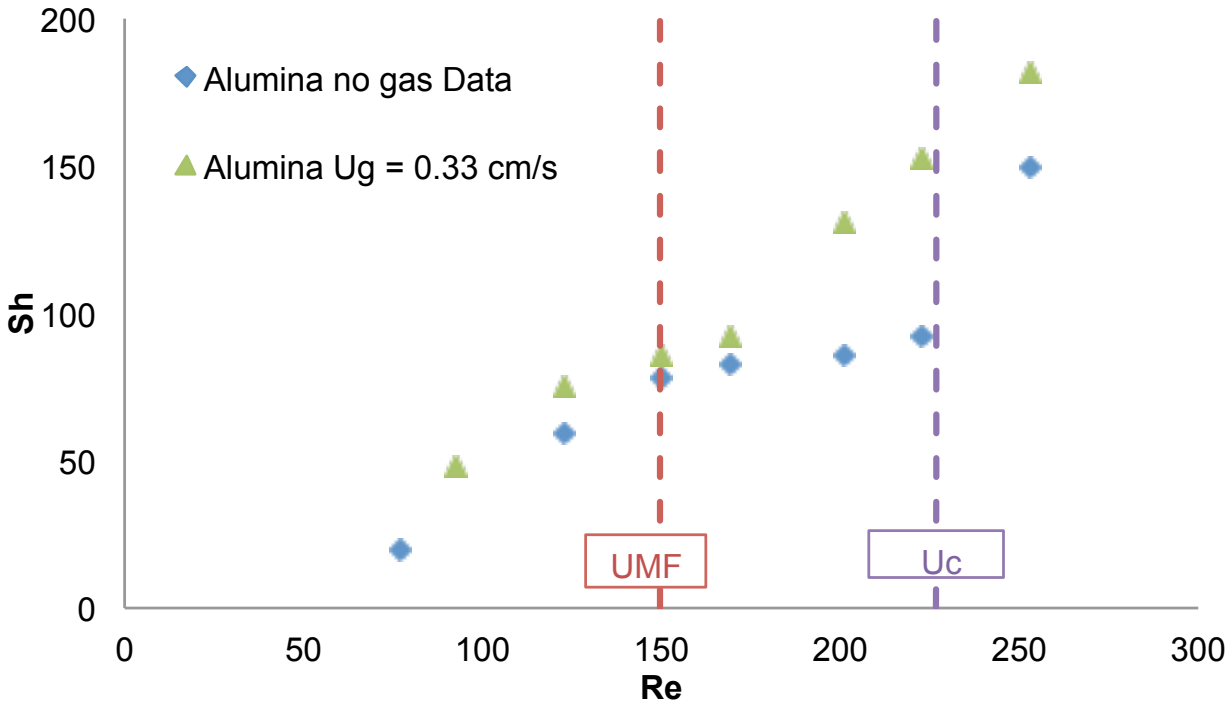

Figure 4.11: Data obtained for liquid-solid mass transfer in two- and three-phase fluidization (superficial gas velocity of 0.33 cm/s) for alumina particles. u_{mf} and u_c values are for the two-phase system

It can be seen in Figure 4.11 that a similar trend was found for both two- and three-phase fluidization with some key differences. The liquid-solid mass transfer is consistently higher when gas is included in the reactor. This trend was expected because the inclusion of gas in the fluidized bed system agitates the particles more and therefore the liquid around the particles is replenished faster. Other authors (Arters and Fan, 1990) have also witnessed the same phenomenon.

It is also noticeable from Figure 4.11 that a less prominent phase change occurs at the minimum fluidization velocity. For two-phase fluidization the mass transfer rate clearly plateaus at u_{mf}, but for the three-phase system this happens gradually and not as sharply. This is due to the fact that for three-phase systems the gas helps with the fluidization and therefore no clear minimum fluidization velocity exists, but instead the fluidization happens more gradually. Similar results were found by Renganathan and Krishnaiah (2003).

What is very interesting to note from Figure 4.11 is that for the three-phase system, a sharp increase in mass transfer is seen similar to the two-phase system. This sharp increase, however, occurs at a lower superficial liquid velocity for the three-phase system. This phenomenon could not be compared to results from the literature because no studies have been done that have gone up to liquid velocities higher that u_c.

In order to model the liquid-solid mass transfer in three-phase systems the same model correlated by Kawase and Moo-Young (1987) was used. As explained earlier, this model makes use of the energy dissipation theory, and in determining the energy dissipation, the energy of the gas-phase is included. As with two-phase modelling, the model only accurately predicts for the window between u_{mf} and u_c.

Because of the high recycling rate in the reactor it was noticed that some of the gas becomes recycled in the recycling line before exiting the reactor. The fraction of gas in the recycling line was measured to be 25% independent of velocity. For this reason, although a constant gas flow rate is fed to the reactor, the superficial velocity of the gas moving through the reactor bed increases when the liquid velocity increases due to the gas fraction in the recycling line. This fact was included in the modelling in order to obtain accurate predictions. Data for the two particles tested along with modelling predictions can be seen in Figures 4.12 and 4.13.

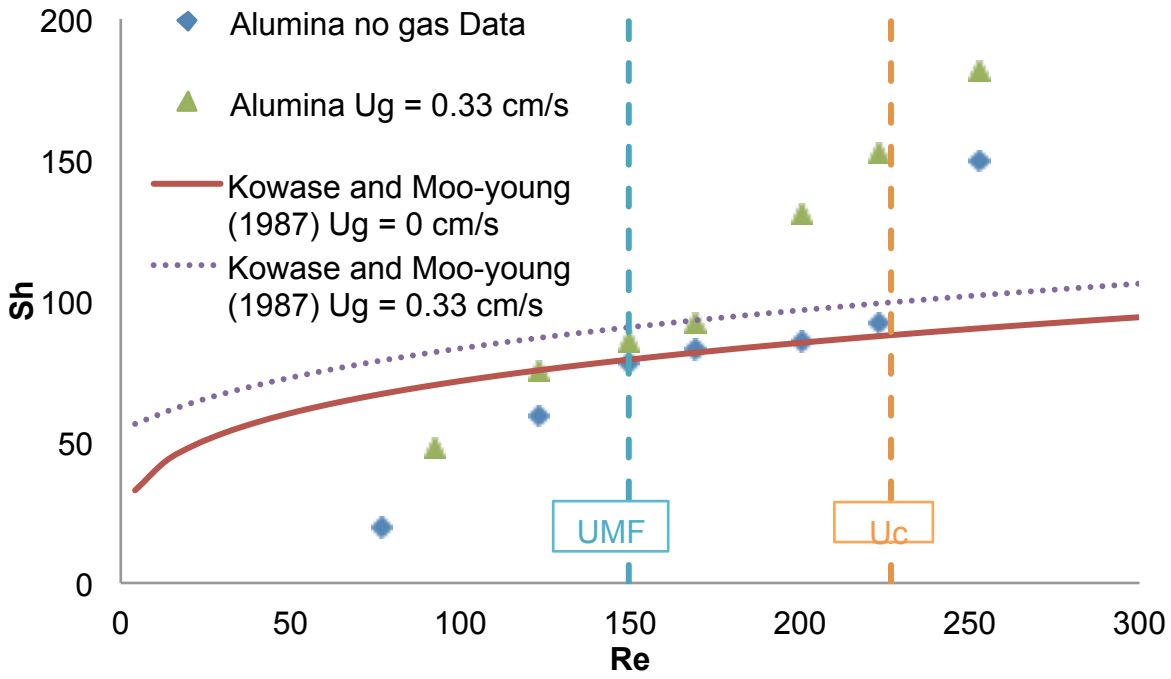

Figure 4.12: Data for two- and three-phase systems with alumina particles along with model predictions from Kawase and Moo-Young (1987). u_{mf} and u_c values are for the two-phase system

It can be seen in Figure 4.13 that the model correlated by Kawase and Moo-Young (1987), with the addition of gas velocity, accurately predicts the data obtained for POM particles, in the window between u_{mf} and u_c. For alumina (Figure 4.12), however, the fit is no longer as good because a sharp increase is seen in the experimental results. The model proposed by Kawase and Moo-Young (1987) did not predict this increase. It is also noticeable that for the POM particles, which have a much lower density than alumina, the increase in mass transfer coefficient with the addition of gas to the system was much higher. An average increase of 52% was achieved in mass transfer for the POM particles. The enhancement of mass transfer by inclusion of gas was much greater for lower-density particles.

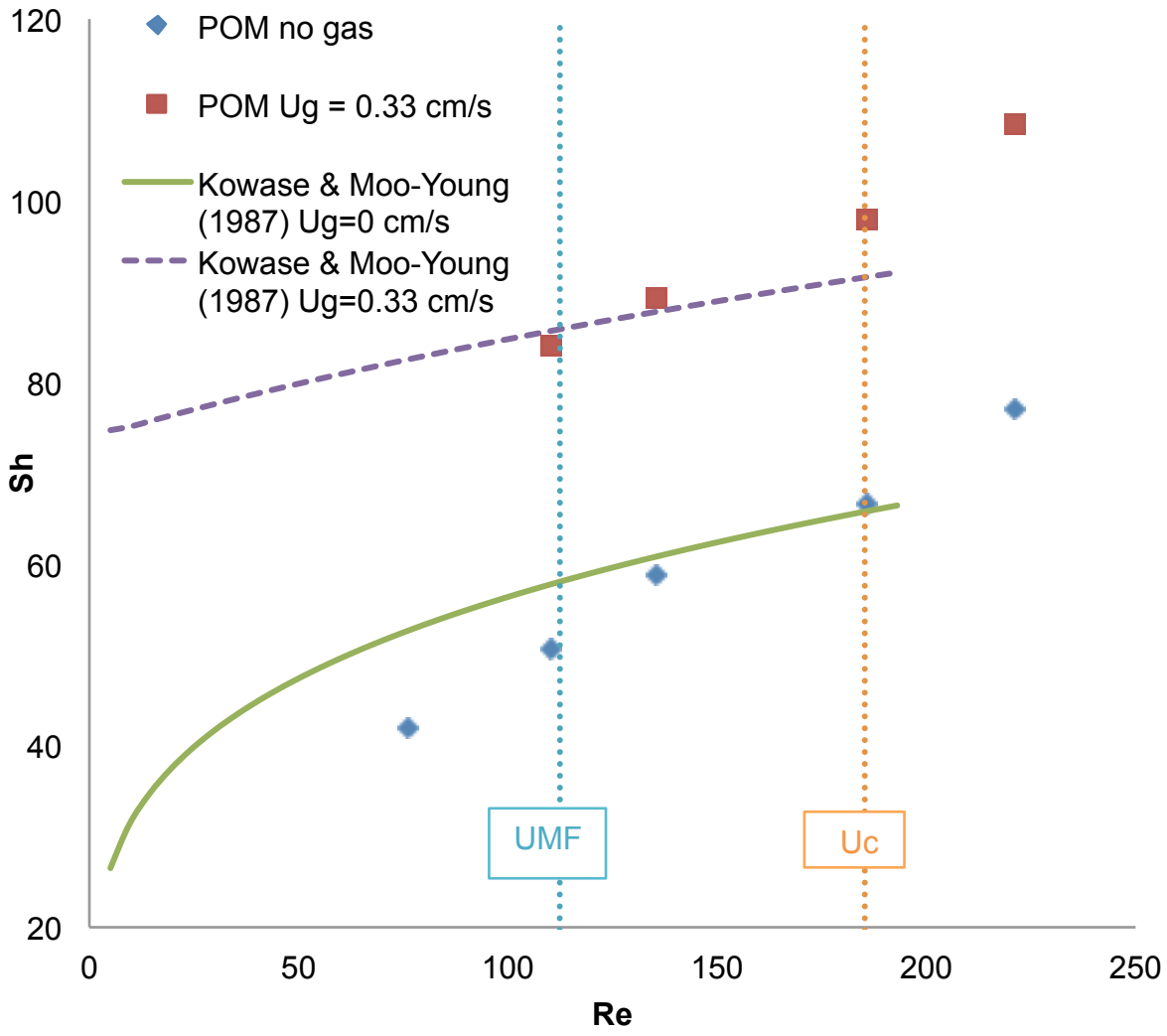

Figure 4.13: Data for two- and three-phase systems with POM particles along with model predictions by Kawase and Moo-Young (1987). u_{mf} and u_c values are for the two-phase system

5. Conclusions

The liquid-solid mass transfer coefficient was experimentally determined in a novel reactor, with external recycling. Liquid-solid experiments were performed in both up- and down-flow mode depending on the particle density. In addition, three-phase experiments were performed in concurrent up-flow mode. The dissolution of benzoic acid method was adapted and used in order to quantify the liquid-solid mass transfer rate. A broader understanding was reached with regard to a number of factors influencing the liquid-solid mass transfer in a reactor and is discussed here.

The liquid-solid mass transfer increased until u_{mf} was reached, after which the increase in mass transfer became slight. This was confirmed to be the minimum fluidization regime. For two of the particles tested (alumina and polypropylene) there exists a liquid velocity (u_c) after which the mass transfer increases sharply. This was deemed the transition to the turbulent regime as seen with gas-solid fluidization; standard u_c correlations were employed to determine this critical velocity for all the particle types. After u_c was reached only a slight increase in mass transfer coefficients was seen for POM and Poraver. No decisive conclusions can be reached on this increase after u_c because it only occurs in two of the four particles.

It was found that the correlation proposed by Kawase and Moo-Young (1987) fits the experimental data from the minimum fluidization velocity (u_{mf}) until the onset of turbulent velocity (u_c) with an AARE of 18%. A new correlation was proposed with the inclusion of the dimensionless group, the Archimedes number. The correlation proposed achieved an AARE of only 8% and can be seen in Equation (5.1).

$$Sh = 0.05Re^{0.42}Sc^{0.66}Ar^{0.17} \quad (5.1)$$

When flow direction in a two-phase fluidized bed was compared, no significant difference was found at similar liquid velocities in liquid-solid mass transfer if the density difference (Δρ) between solid and liquid phases is the same. It can be concluded that the direction of liquid flow has no influence on liquid-solid mass transfer for two-phase fluidized beds. It was, however, found that density difference

(Δρ) has a significant influence on the liquid-solid mass transfer. For a higher Δρ, higher mass transfer coefficients were achieved mainly because of the higher Re numbers required to achieve fluidization.

The experimental results obtained for packed bed liquid-solid mass transfer compared well with the model proposed by Thoenes and Kramers (1959). A comparison between fluidized bed and packed bed liquid-solid mass transfer showed that the Archimedes number (driven by density difference) had a major influence. When Δρ is high, as for the alumina particles (Δρ = 1300 kg/m^3), the fluidized bed outperforms the packed bed (Sh_{FB}/Sh_{PB} = 1.25). When the density difference becomes smaller, Δρ = 580 kg/m^3, the fluidized bed only slightly outperforms the packed bed setup. For a very small density difference (Δρ = -145 kg/m^3) the packed bed substantially outperforms the fluidized bed (Sh_{FB}/Sh_{PB} = 0.7). It was also noted that the Sherwood ratio was not significantly dependent on the liquid velocity.

When liquid-solid mass transfer rates were determined for three-phase systems only up-flow could be compared. The introduction of gas improves the liquid-solid mass transfer at the same liquid velocity when two-phase and three-phase systems are compared. It was also found that no significant transitions were seen between the flow regimes as seen with two-phase fluidization. This was because a gradual fluidization occurred with three-phase fluidization and not instantaneous fluidization as with liquid-solid fluidized beds. The enhancement of mass transfer by inclusion of gas was more severe for lower-density particles.

6. References

Arters, D. C. and Fan, L.S. (1986) “Solid-liquid mass transfer in a gas-liquid-solid fluidized bed” *Chemical Engineering Science*, 41, 107-115.

Arters, D.C. and Fan, L (1990) “Experimental methods and correlation of solid-liquid mass transfer in fluidized beds” *Chemical Engineering Science,* 45, 965-975.

Asai, A., Konishi, Y. and Maeda, H. (1985) *Chem Eng Sci 40,* 1573.

Banerjee, J. Basu, J.K. and Ganguly, U.P. (1999) “Some studies on the hydrodynamics of reverse fluidization velocities*”, Ind. Chem. Eng. 41* (1) 35–38.

Behkish, A., Lemoine, R., Oukaci, R. and Morsi, B.I. (2006) “Novel correlations for gas holdup in large-scale slurry bubble column reactors operating under elevated pressures and temperatures”, *Chem. Eng. J.,* 115, 157–171.

Biswas, S.K. and Ganguly, U.P. (1997) “A preliminary study on the voidage–velocity relationship in reverse fluidization”, *Ind. Chem. Eng., 39,* 303–306.

Buffière, P and Moletta, R. (1999) “Some hydrodynamic characteristics of inverse three phase fluidized-bed reactors”, *Chem. Eng. Sci.,* 54, 1233–1242.

Calderon, D.G., Buffiere, P., Moletta, R. and Elmaleh, S. (1998) “Anaerobic digestion of wine distillery wastewater in down-flow fluidized bed”, *Wat. Res. 32,* 3593–3600.

Cho, Y.J., Park, H.Y., Kim, S.W., Kang, Y. and Kim, S.D.(2002) “Heat transfer and hydrodynamics in two- and three-phase inverse fluidized beds” *Ind. Eng. Chem. Res*., 41, 2058–2063.

Deckwer, W.D. (1980) *Chem Eng Sci 35,* 1341.

Delgado, J. M. P. Q. (2006) “Experimental data of solubility at different temperatures: a simple technique”, Springer-Verlag.

Fan, L, Muroyama, K and Chern, S (1982) “Hydrodynamic characteristics of inverse fluidization in liquid-solid and gas-liquid-solid systems”, *Chemical Engineering Journal,* 24, 143-150.

Fan, L.S., (1989) “Gas–liquid–solid fluidization engineering”, Butterworths, Stoneham.

Fogler, H. S., (2009) “Elements of chemical reaction engineering”, prentice-hall, englewood cliffs, New Jersey.

Fukuma, M., Sato, M., Muroyama, K. and Yasunishi, A., (1988) “Particle-to-liquid mass transfer in gas-liquid-solid fluidization”, *J. Chem. Engng Japan,* 21, 231-237.

Gamson B. W., (1951) “Heat and mass transfer (liquid solid systems)”. *Chem. Engng Prog,* 47, 19-28.

Hassanien, S., Delmas, H. and Riba, J. P. (1984) “Transfert de matière liquid”, *Particules Entropie,* 119, 17-26.

Ibrahim, Y. A. A., Briens, C. L., Margaritis, A. and Bergongnou, M. A. (1996) “Hydrodynamic characteristics of a 3-phase inverse fluidized bed column”, *AIChE Journal*, *42*, 1889–1900.

Kawase, Y. and Moo-Young, M. (1987) “Solid-turbulent fluid heat and mass transfer: a unified model based on the energy dissipation rate concept”, *Chem. Engng J. 36,3140.*

Khan, A.R. and Richardson, J.F. (1990) “Pressure gradient and friction factor for sedimentation and fluidization of uniform spheres in liquids”, *Chemical Engineering Science,* 45, 255–265.

Kikuchi, K., Suaawara. T. and Ohashi. H. (1983) “Correlation of mass transfer coefficient between particles and liquid in liquid fluidized beds”, *J. Chem. Engng Japan, 16, 426428.*

Kim, S.D. and Kang, Y. (1997) “Heat and mass transfer in three-phase fluidized-bed reactor - an overview”, *Chemical Engineering Science, 52,* 3639–3660.

Krishnaiah, K., Guru, S. and Sekar, V. (1993) “Hydrodynamic studies on inverse gas–liquid–solid fluidization*”, Chemical Engineering Journal, 51, 109–112.*

Kunii, D. and Levenspiel, O. (1999) *Fluidization engineering*, Butterworth-Heinemann, London, Boston.

Lee, K. W. and Kim, J. C. (1990) “Experimental study of particle collection by small cyclones”, *Aerosol Science and Technology,* 12, 1005 -1015.

Legile, P., Menard, G., Laurent, C., Thomas, D. and Bernis, A. (1992) “Contribution to the study of an inverse 3-phase fluidized bed operating countercurrently”, *International Chemical Engineering*, *32*, 41–50.

Myre, D. and Macchi, A. (2010) “Heat transfer and bubble dynamics in a three-phase inverse fluidized bed”, *Chemical Engineering and Processing*, 49, 523-529.

Nakajima, M., Harada, M., Asai, M., Yamazaki, R. and Jimbo, G. (1991) “Bubble fraction and voidage in an emulsion phase in the transition to a turbulent fluidized bed”, Circulating Fluidized Bed III (pp. 79-84). Oxford: Pergamon Press.

Nikolov, L. and Karamanev, D. (1987) “Experimental study of the inverse fluidized bed biofilm reactor”, *Can. J. Chem. Eng.,* 65, 214–217.

Nikov, I. and Delmas, H. (1987) “Solid-liquid mass transfer in three-phase fixed and fluidized beds”, *Chemical Engineering Science,* 42, 1089-1093.

Niven, R.K. (2002) “Physical insight into the Ergun and Wen & Yu equations for fluid flow in packed and fluidized beds”, *Chemical Engineering Science, 57*, 527-534.

Prakash, A., Briens, C. L. and Bergougnou, M. A. (1987) “Mass transfer between solid particles and liquid in a three phase fluidized bed”, *Can. J. Chem. Eng,* 65, 228-236.

Qing-Zhu, J., Pei-Sheng, M., Huan, Z., Shu-Qian, X., Qiang, W. and Yan, Q. (2006) “The effect of temperature on the solubility of benzoic acid derivatives in water”, College of Chemical Engineering, Tianjin University, Tianjin 300072, P.R. China.

Renganathan, T. and Krishnaiah, K. (2003) “Prediction of minimum fluidization velocity in two and three phase inverse fluidized beds”, *Can. J. Chem. Eng.,* 81, 853–860.

Renganathan, T. and Krishnaiah, K. (2004) “Liquid phase mixing in 2-phase liquid-solid inverse fluidized bed”, *Chemical Engineering Journal*, 98, 213-218.

Renganathan, T. and Krishnaiah, K. (2005) “Voidage characteristics and prediction of bed expansion in liquid-solid inverse fluidized bed”, *Chemical Engineering Science,* 60, 2545-2555.

Richardson, J. F. and Zaki, W. N. (1954) “Sedimentation and fluidization: Part I”, *Trans. Inst. Chem. Eng.,* 32, 3553.

Roy, S. and Dudukovic, M.P., (2001) “Flow mapping and modelling of liquid–solid risers”, *Industrial and Engineering Chemistry Research, 40,* 5440–5454.

Sanger, P. and Deckwer, W.D. (1981) *Chem Eng J, 22,* 179.

Sano, Y.N., Yamaguchi, N. and Adachi, T. (1974) *Chem Eng Jpn 1,* 255.

Shen, G.C., Geankoplis, C.J. and Brodkey, R.S. (*1985)* “A note on particle-liquid mass transfer in a fluidized bed of small irregular-shaped benzoic acid particles”, *Chemical Engineering Science*, *40: 9*, *1797-1802.*

Son, S.M., Kang, S.H., Kim, U.Y., Kang, Y. and Kim, S.D. (2007) “Bubble properties in three-phase inverse fluidized beds with viscous liquid medium”, *Chem. Eng. Process*, 46, 736–741.

Thoenes, D. and Kramers, H. (1958) “Mass transfer from spheres in various regular packings to a flowing fluid”, *Chemical Engineering Science 8*, 271-283.

Turton, R. and Clark, N.N. (1987) “An explicit relationship to predict spherical particle velocity”, *Powder Technology,* 53, 127–129.

Ulaganathan, N. and Krishnaiah, K. (1996) “Hydrodynamic characteristics of two-phase inverse fluidized bed”, *Bioprocess Eng, 15*:159–164.

Vijayalakshmi, A.C., Balamurugan, M, Sivakumar, M., Samuel, T.N. and Velan, M. (2000) “Minimum fluidization velocity and friction factor in a liquid-solid inverse fluidized bed reactor”, *Bioprocess Biosys Eng,* 22:461–466.

Wen, C.Y. and Yu, Y.H. (1966) “Mechanics of fluidization”, *Chem. Eng. Prog. Symposium Series,* 66, 101–111.

Yang, X.L., Wild, G. and Euzen, J.P. (1993) “Study of liquid retention in fixed- bed reactors with upward flow of gas and liquid”, *Int. Chem. Eng*. 33, 72–84.

Zhang, J.P., Epstein, N., Grace J.R. and Zhu, J. (1995) “Minimum liquid fluidization velocity of gas–liquid fluidized beds”, *Trans. IchemE*. 73, 347–353.

7. Appendices

7.1 Appendix A: Analytical calibrations

Before starting with the experiment, a number of calibrations had to be done on the peristaltic pumps, the voltage probe and the data acquisition system. Firstly the two pumps were calibrated by setting the RPM and measuring the flow rate. A fit was then done in order to find the relationship that could be used in future. In Figure 7.1 below the calibration curves can be seen, and the two equations that describe the relationship between flow rate (Q) and RPM can be seen in Equation (7.1) (for the blue pump) and Equation (7.2) (for the green pump).

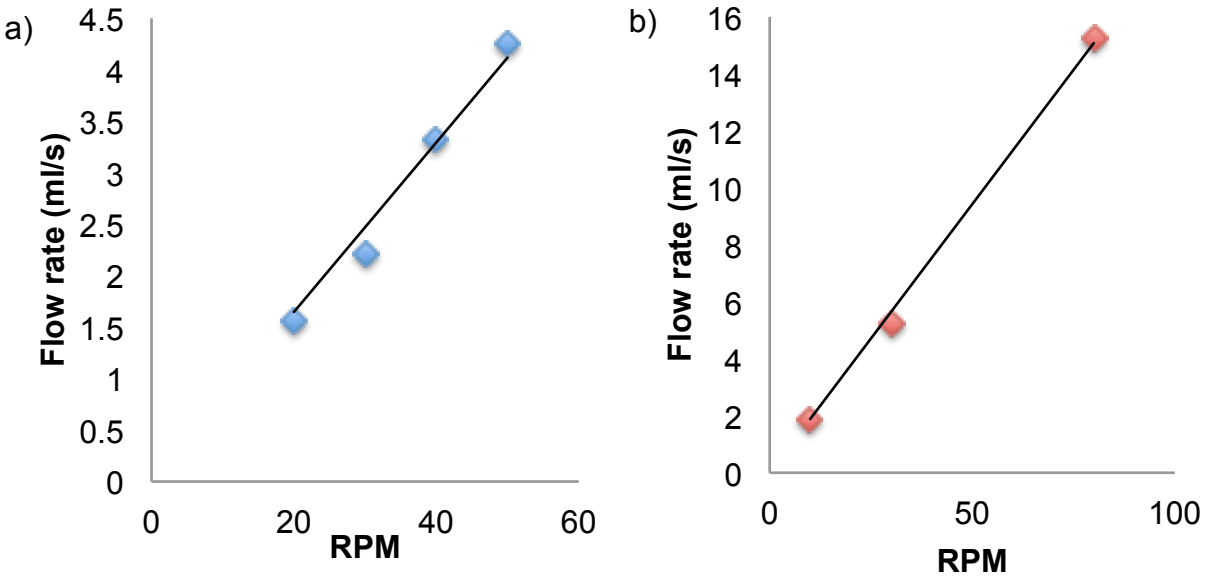

Figure 7.1: a) Calibration curve for the blue pump (Watson Merlow 323), b) calibration curve for the green pump (Watson Merlow 520S pump).

$$Q = 0.0823 \times \mathrm{RPM} \quad (7.1)$$

$$Q = 0.1885 \times \mathrm{RPM} \quad (7.2)$$

In order to use the dissolution of benzoic acid method, apparatus was needed to accurately measure the benzoic acid concentration in solution over time during an experimental run. A UV spectrometer was chosen, but before it could be used accurately, a number of calibration experiments had to be done in order to find the best light wavelength and to determine the relationship between the measured absorbance (A) and the required concentration (C).

From results of previous studies, a wavelength of 293 nm was found to give a straight-line relationship between concentration and absorbance. This wavelength was therefore used in all further measurements.

A number of samples of known concentration were prepared and placed in the UV spectrometer. The measured absorbance of each sample was tabulated along with the concentrations and a plot was drawn. The results can be seen in Figure 7.2. A trend line was fitted to the results and a relationship was found, which can be seen in Equation (7.3).

$$C = 4.942\ A \tag{7.3}$$

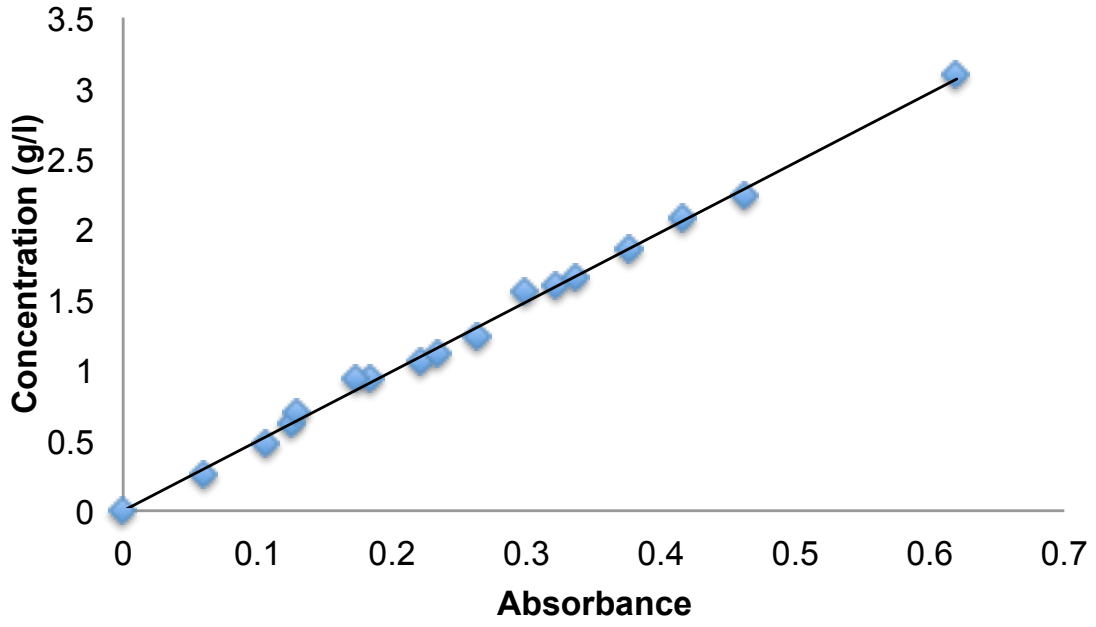

Figure 7.2: Concentration versus absorbance calibration curve

7.2 Appendix B: Liquid-solid mass transfer plots

In order to optimize the sampling technique, data collection and the efficiency of the experiments, the experimental method was applied to different reactor setups to compare them regarding liquid-solid mass transfer. Four different particles were used and the experiment was done in a stagnant beaker reactor (batch), a stirred beaker reactor (stir) and a fluidized reactor. Because two of the four particles have a higher density than water, these were tested while running the fluidized bed in classical fluidization mode. The other two particles have densities lower than that of water and for them the bed was run in inverse fluidization mode.

All the experimental data were plotted and predictions were made with the model in order to compile the liquid-solid mass transfer coefficient for all four particle types in all three reactor setups. Figure 7.3 is an example of the results obtained.

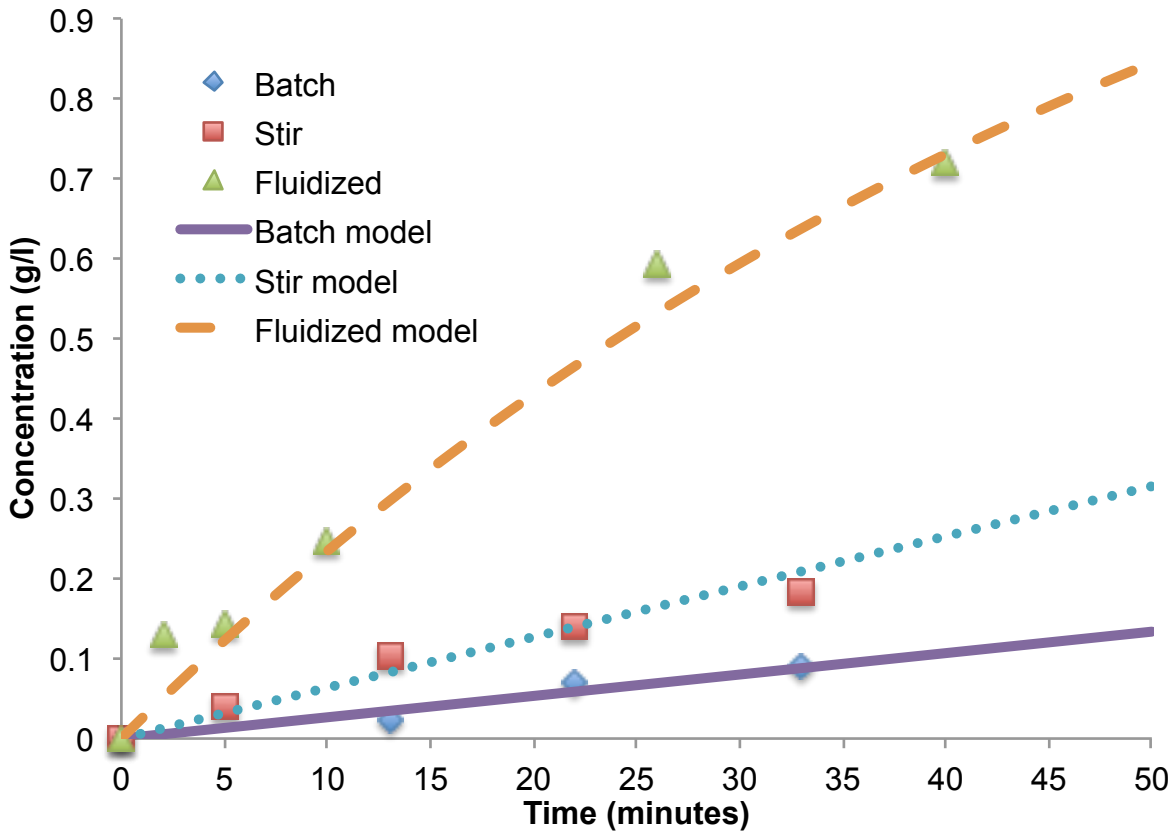

Figure 7.3: Experimental data along with model predictions for the dissolution of benzoic acid coated on 3.5 mm alumina particles in three different reactor setups

It can be seen in Figure 7.3 that, as expected, the batch run had the worst mass transfer because the liquid is stationary and therefore the concentration gradient around the particles is not refreshed with new water. For the stirred reactor setup the beaker with the water and the particles was placed inside an orbital shaker and set to 200 RPM. Because the whole beaker is shaken the mixing of the water is better but still not excellent. It can be seen that the fluidized reactor gave the best mass transfer results. Some more examples of the fits done to determine mass transfer coefficients can be seen in Figures 7.4 and 7.5.

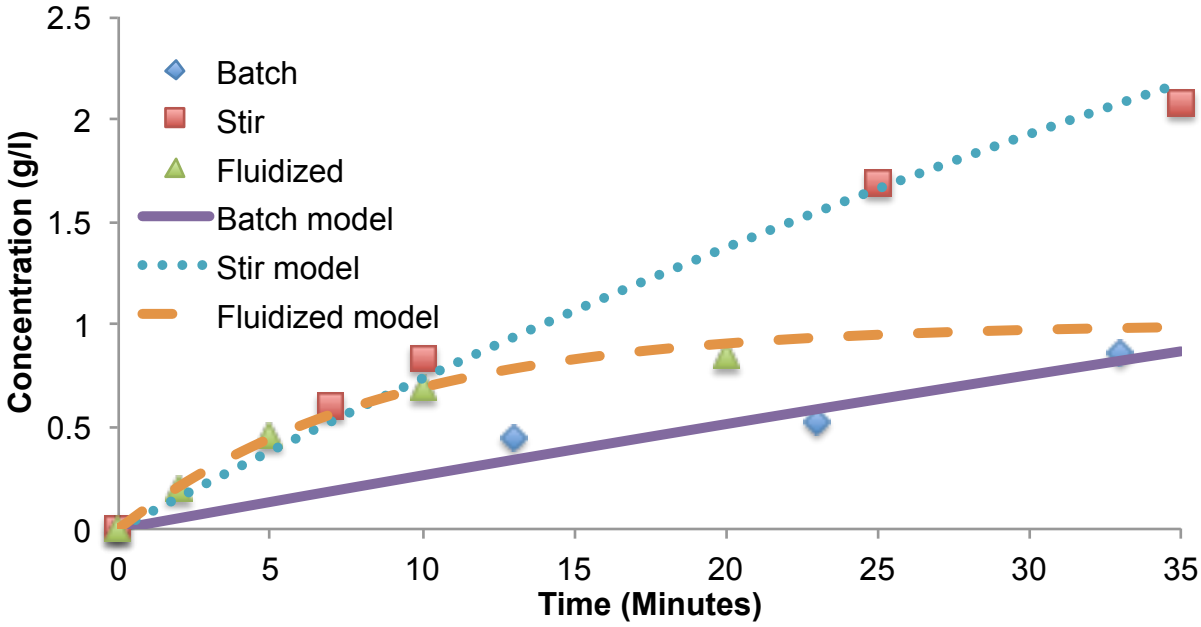

Figure 7.4: Experimental data along with model predictions for the dissolution of benzoic acid coated on polypropylene particles in three different reactor setups

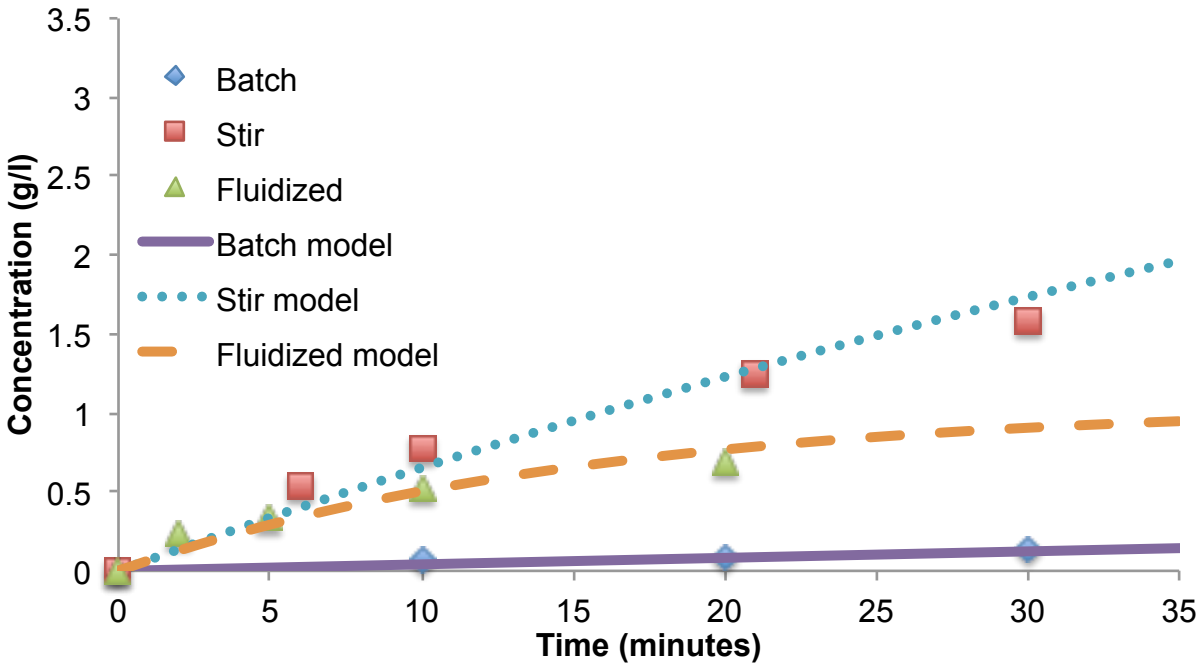

Figure 7.5: Experimental data along with model predictions for the dissolution of benzoic acid coated on Poraver particles in three different reactor setups

7.3 Appendix C: Expanded drawing of fluidized bed reactor